Inorg. Chem. **2004**, *43*, 7441–7455

Alkyl- and Aryl-Substituted Corroles. 5. Synthesis, Physicochemical Properties, and X-ray Structural Characterization of Copper Biscorroles and Porphyrin–Corrole Dyads

Roger Guilard,* Claude P. Gros, Jean-Michel Barbe, Enrique Espinosa, François Jérôme,† and Alain Tabard

Université de Bourgogne, LIMSAG UMR 5633, Faculté des Sciences Gabriel, 6, boulevard Gabriel, 21000-Dijon, France

Jean-Marc Latour

CEA Grenoble, Laboratoire DRDC/PMB, UMR 5155 CEA-CNRS-UJF, 38056-Grenoble Cedex 09, France

Jianguo Shao, Zhongping Ou, and Karl M. Kadish*

University of Houston, Department of Chemistry, Houston, Texas 77204-5003

Received March 16, 2004

The synthesis and characterization of cofacial copper biscorroles and porphyrin–corroles linked by a biphenylenyl or anthracenyl spacer are described. The investigated compounds are represented as (BCA)Cu_2 and (BCB)Cu_2 in the case of the biscorrole (BC) derivatives and (PCA)Cu_2 and (PCB)Cu_2 in the case of porphyrin (P)–corrole (C) dyads, where A and B represent the anthracenyl and biphenylenyl bridges, respectively. A related monomeric corrole (Me_4Ph_5Cor)Cu and monomeric porphyrin (Me_2Et_6PhP)Cu that comprise the two halves of the porphyrin–corrole dyads were also studied. Electron spin resonance (ESR), ^{1}H NMR, and magnetic measurements data demonstrate that the copper corrole macrocycle, when linked to another copper corrole or copper(II) porphyrin, can be considered to be a Cu(III) complex in equilibrium with a Cu(II) radical species, copper(III) corrole being the main oxidation state of the corrole species at all temperatures. The cofacial orientation of (BCB)Cu_2, (BCA)Cu_2, and (PCB)Cu_2 was confirmed by X-ray crystallography. Structural data: (BCB)Cu_2($C_{110}H_{82}N_8Cu_2$·3$CDCl_3$), triclinic, space group $P\bar{1}$, a = 10.2550(2) Å, b = 16.3890(3) Å, c = 29.7910(8) Å, α = 74.792(1)°, β = 81.681(1)°, γ = 72.504(2)°, Z = 2; (BCA)Cu_2·($C_{112}H_{84}N_8Cu_2$·C_7H_8·1.5H_2O), monoclinic, space group $P\,2_1/c$, a = 16.0870(4) Å, b = 35.109(2) Å, c = 19.1390(8) Å, β = 95.183(3)°, Z = 4; (PCB)Cu_2($C_{89}H_{71}N_8Cu_2$·$CHCl_3$), monoclinic, space group $P2_1/n$, a = 16.7071(3) Å, b = 10.6719(2) Å, c = 40.8555(8) Å, β = 100.870(1)°, Z = 4. The two cofacial biscorroles, (BCA)Cu_2 and (BCB)Cu_2, both show three electrooxidations under the same solution conditions. The reduction of (BCA)Cu_2 involves a reversible electron addition to each macrocycle at the same potential of $E_{1/2}$ = –0.20 V although (BCB)Cu_2 is reversibly reduced in two steps to give first $[(BCB)Cu_2]^-$ and then $[(BCB)Cu_2]^{2-}$, each of which was characterized by ESR spectroscopy as containing a Cu(II) center. These latter electrode reactions occur at $E_{1/2}$ = –0.36 and –0.51 V versus a saturated calomel reference electrode. The half-reduced and fully reduced (BCB)Cu_2 show similar Cu(II) ESR spectra, and no evidence of a triplet signal is observed. The two well-separated reductions of (BCB)Cu_2 to give $[(BCB)Cu_2]^{2-}$ can be attributed to a stronger π–π interaction between the two macrocycles of this dimer as compared to those of (BCA)Cu_2. The copper porphyrin–corrole dyads, (PCA)Cu_2 and (PCB)Cu_2, show five reversible oxidations and two reversible reductions, and these potentials are compared with corresponding values for electrochemical reactions of the porphyrin and corrole monomers under the same solution conditions.

Introduction

The last 10 years have shown a renaissance of interest in the study of corroles and metallocorroles that were first reported in the mid 1960s[1–3] but not investigated in any detail until several facile syntheses for the preparation of these compounds had become available.[4–23] The first attempts to

* Authors to whom correspondence should be addressed. E-mail: Roger.Guilard@u-bourgogne.fr (R.G.); kkadish@uh.edu (K.M.K.).

† Present address: Université de Poitiers, LACCO-ESIP, UMR 6503 CNRS, 40, avenue du Recteur Pineau, 86022 Poitiers, France.

(1) Johnson, A. W.; Kay, I. T. *J. Chem. Soc.* **1965**, 1620−1629.
(2) Johnson, A. W.; Kay, I. T. *Proc. R. Soc. London, Ser. A* **1965**, *288*, 334−341.
(3) Johnson, A. W.; Kay, I. T. *Proc. Chem. Soc., London* **1964**, 89−90.

10.1021/ic049651c CCC: $27.50
Published on Web 10/22/2004

synthesize corroles with many different transition-metal ions were carried out by Boschi and co-workers[24−26] using octamethyl derivatives, and this was followed several years later by detailed studies of complexes with other macrocycles such as octaethylcorroles,[27−33] pentafluorotriphenyl corroles,[11,12,34−38] and triarylcorroles,[10,14−16,39,40] thus establishing a good database of information on corroles with different metal ions and different macrocycles.

Our own research interest has been directed toward the study of aryl-substituted corroles in their mononuclear or binuclear form.[4,41−48] These latter compounds can be linked via one of several different spacer groups to give face-to-face dyads.[41−47] One key interest of these dyads is their ability to bind small molecules such as CO or nitrogenous bases,[41,42,44] and another is the interaction that can occur between the two corrole units as has often been seen for similar linked bisporphyrins.[4,49,50] Furthermore, we have been able to synthesize heterobimetallic dyads where a porphyrin and a corrole are linked together in a cofacial arrangement by a rigid spacer.[41,44−46,51] These porphyrin−corrole derivatives have the possibilities for displaying versatile complexation properties whereas both mono- and bimetallic complexes have been isolated.[41,44−46,51] Monocobalt derivatives with the cobalt atom inside the corrole moiety can be easily obtained, thus allowing for the further insertion of a large variety of metals into the porphyrin macrocycle.[51]

This paper describes the synthesis, structural characterization, and properties of four homobimetallic copper dyads represented as (BCA)Cu_2 and (BCB)Cu_2 in the case of biscorrole derivatives and (PCA)Cu_2 and (PCB)Cu_2 in the case of porphyrin (P)−corrole (C) dyads, where A and B represent the anthracenyl and biphenylenyl bridges, respectively (Chart 1). This work builds upon earlier studies involving cobalt complexes of bisporphyrins,[49] biscorroles,[41,42,45,47] and porphyrin−corrole dyads.[41,44−46] The properties of the herein reported face-to-face linked metallomacrocycles that can exhibit interaction between the two macrocycles are monitored by several spectroscopic techniques, X-ray diffraction, and electrochemistry.

The synthesis and characterization of a related copper monocorrole, (Me_4Ph_5Cor)Cu, and a copper monoporphyrin,

(4) Guilard, R.; Barbe, J. M.; Stern, C.; Kadish, K. M. In *The Porphyrin Handbook*; Kadish, K. M., Smith, K. M., Guilard, R., Eds.; Elsevier: New York, 2003; Vol. 116, pp 303−348.
(5) Decréau, R. A.; Collman, J. P. *Tetrahedron Lett.* **2003**, *44*, 3323−3327.
(6) Paolesse, R. In *The Porphyrin Handbook*; Kadish, K. M., Smith, K. M., Guilard, R., Eds.; Academic Press: New York, 2000; Vol. 2, pp 201−232.
(7) Erben, C.; Will, S.; Kadish, K. M. In *The Porphyrin Handbook*; Kadish, K. M., Smith, K. M., Guilard, R., Eds.; Academic Press: New York, 2000; Vol. 2, pp 233−300.
(8) Genokhova, N. S.; Melent'eva, T. A.; Berezovskii, V. M. *Russ. Chem. Rev.* **1980**, *49*, 1056−1067.
(9) Melent'eva, T. A. *Russ. Chem. Rev.* **1983**, *52*, 641−661.
(10) Gryko, D. T. *Eur. J. Org. Chem.* **2002**, 1735−1743.
(11) Gross, Z.; Galili, N.; Saltsman, I. *Angew. Chem., Int. Ed.* **1999**, *38*, 1427−1429.
(12) Gross, Z.; Galili, N.; Simkhovich, L.; Saltsman, I.; Botoshansky, M.; Blaeser, D.; Boese, R.; Goldberg, I. *Org. Lett.* **1999**, *1*, 599−602.
(13) Gryko, D. T.; Koszarna, B. *Org. Biomol. Chem.* **2003**, *1*, 350−357.
(14) Gryko, D. T. *J. Chem. Soc., Chem. Commun.* **2000**, 2243−2244.
(15) Gryko, D. T.; Jadach, K. *J. Org. Chem.* **2001**, *66*, 4267−4275.
(16) Gryko, D. T.; Piechota, K. E. *J. Porphyrins Phthalocyanines* **2002**, 81−97.
(17) Steene, E.; Dey, A.; Ghosh, A. *J. Am. Chem. Soc.* **2003**, *125*, 16300−16309.
(18) Paolesse, R.; Pandey, R. K.; Forsyth, T. P.; Jaquinod, L.; Gerzevske, K. R.; Nurco, D. J.; Senge, M. O.; Licoccia, S.; Boschi, T.; Smith, K. M. *J. Am. Chem. Soc.* **1996**, *118*, 3869−3882.
(19) Paolesse, R.; Nardis, S.; Sagone, F.; Khoury, R. G. *J. Org. Chem.* **2001**, *66*, 550−556.
(20) Paolesse, R.; Macagnano, A.; Monti, D.; Tagliatesta, P.; Boschi, T. *J. Porphyrins Phthalocyanines* **1998**, *2*, 501−510.
(21) Paolesse, R.; Jaquinod, L.; Nurco, D. J.; Mini, S.; Sagone, F.; Boschi, T.; Smith, K. M. *J. Chem. Soc., Chem. Commun.* **1999**, 1307−1308.
(22) Neya, S.; Ohyama, K.; Funasaki, N. *Tetrahedron Lett.* **1997**, *38*, 4113−4116.
(23) Lee, C.-H.; Cho, W.-S.; Ka, J.-W.; Kim, H.-J.; Lee, P. H. *Bull. Chem. Soc. Jpn.* **2000**, *21*, 429−433.
(24) Boschi, T.; Licoccia, S.; Paolesse, R.; Tagliatesta, P. *Inorg. Chim. Acta* **1988**, *141*, 169−171.
(25) Boschi, T.; Licoccia, S.; Paolesse, R.; Tagliatesta, P.; Azarnia Tehran, M.; Pelizzi, G.; Vitali, F. *J. Chem. Soc., Dalton Trans.* **1990**, 463−468.
(26) Kadish, K. M.; Koh, W.; Tagliatesta, P.; Sazou, D.; Paolesse, R.; Licoccia, S.; Boschi, T. *Inorg. Chem.* **1992**, *31*, 2305−2313.
(27) Autret, M.; Will, S.; Caemelbecke, E. V.; Lex, J.; Gisselbrecht, J.-P.; Gross, M.; Vogel, E.; Kadish, K. M. *J. Am. Chem. Soc.* **1994**, *116*, 9141−9149.
(28) Van Caemelbecke, E.; Will, S.; Autret, M.; Adamian, V. A.; Lex, J.; Gisselbrecht, J.-P.; Gross, M.; Vogel, E.; Kadish, K. M. *Inorg. Chem.* **1996**, *35*, 184−192.
(29) Will, S.; Lex, J.; Vogel, E.; Adamian, V. A.; Van Caemelbecke, E.; Kadish, K. M. *Inorg. Chem.* **1996**, *35*, 5577−5583.
(30) Kadish, K. M.; Adamian, V. A.; Van Caemelbecke, E.; Gueletii, E.; Will, S.; Erben, C.; Vogel, E. *J. Am. Chem. Soc.* **1998**, *120*, 11986−11993.
(31) Kadish, K. M.; Will, S.; Adamian, V. A.; Walther, B.; Erben, C.; Ou, Z.; Guo, N.; Vogel, E. *Inorg. Chem.* **1998**, *37*, 4573−4577.
(32) Kadish, K. M.; Ou, Z.; Adamian, V. A.; Guilard, R.; Gros, C. P.; Erben, C.; Will, S.; Vogel, E. *Inorg. Chem.* **2000**, *39*, 5675−5682.
(33) Kadish, K. M.; Erben, C.; Ou, Z.; Adamian, V. A.; Will, S.; Vogel, E. *Inorg. Chem.* **2000**, *39*, 3312−3319.
(34) Gross, Z.; Simkhovich, L.; Galili, N. *J. Chem. Soc., Chem. Commun.* **1999**, 599−600.
(35) Gross, Z.; Galili, N. *Angew. Chem., Int. Ed. Engl.* **1999**, *38*, 2366−2369.
(36) Gross, Z.; Simkhovich, L.; Nitsa, G. N.; Saltsman, I. WO 00/18771, 2000.
(37) Gross, Z.; Golubkov, G.; Simkhovich, L. *Angew. Chem., Int. Ed.* **2000**, *39*, 4045−4047.
(38) Luobeznova, I.; Simkhovich, L.; Goldberg, D. P.; Gross, Z. *Eur. J. Inorg. Chem.* **2004**, 1724−1732.
(39) Brückner, C.; Brinas, R. P.; Bauer, J. A. K. *Inorg. Chem.* **2003**, *42*, 4495−4497.
(40) Brückner, C.; Barta, C. A.; Brinas, R. P.; Bauer, J. A. K. *Inorg. Chem.* **2003**, *42*, 1673−1680.
(41) Kadish, K. M.; Ou, Z.; Shao, J.; Gros, C. P.; Barbe, J.-M.; Jérôme, F.; Bolze, F.; Burdet, F.; Guilard, R. *Inorg. Chem.* **2002**, *41*, 3990−4005.
(42) Guilard, R.; Jérôme, F.; Barbe, J.-M.; Gros, C. P.; Ou, Z.; Shao, J.; Fischer, J.; Weiss, R.; Kadish, K. M. *Inorg. Chem.* **2001**, *40*, 4856−4865.
(43) Guilard, R.; Gros, C. P.; Bolze, F.; Jérôme, F.; Ou, Z.; Shao, J.; Fischer, J.; Weiss, R.; Kadish, K. M. *Inorg. Chem.* **2001**, *40*, 4845−4855.
(44) Guilard, R.; Jérôme, F.; Gros, C. P.; Barbe, J.-M.; Ou, Z.; Shao, J.; Kadish, K. M. *C. R. Acad. Sci., Ser. IIc: Chim.* **2001**, *4*, 245−254.
(45) Jérôme, F.; Barbe, J.-M.; Gros, C. P.; Guilard, R.; Fischer, J.; Weiss, R. *New J. Chem.* **2001**, *25*, 93−101.
(46) Jérôme, F.; Gros, C. P.; Tardieux, C.; Barbe, J. M.; Guilard, R. *New J. Chem.* **1998**, *22*, 1327−1329.
(47) Jérôme, F.; Gros, C. P.; Tardieux, C.; Barbe, J. M.; Guilard, R. *J. Chem. Soc., Chem. Commun.* **1998**, 2007−2008.
(48) Tardieux, C.; Gros, C. P.; Guilard, R. *J. Heterocycl. Chem.* **1998**, *35*, 965−970.
(49) Collman, J. P.; Boulatov, R.; Sunderland, C. J. In *The Porphyrin Handbook*; Kadish, K. M., Smith, K. M., Guilard, R., Eds.; Elsevier: New York, 2003; Vol. 62, pp 1−45.
(50) Barbe, J. M.; Guilard, R. In *The Porphyrin Handbook*; K. M. Kadish, K. M. Smith, Guilard, R., Eds.; Academic Press: New York, 2000; Vol. 3, p 211−241.
(51) Barbe, J.-M.; Burdet, F.; Espinosa, E.; Gros, C. P.; Guilard, R. *J. Porphyrins Phthalocyanines* **2003**, *7*, 365−374.

Chart 1

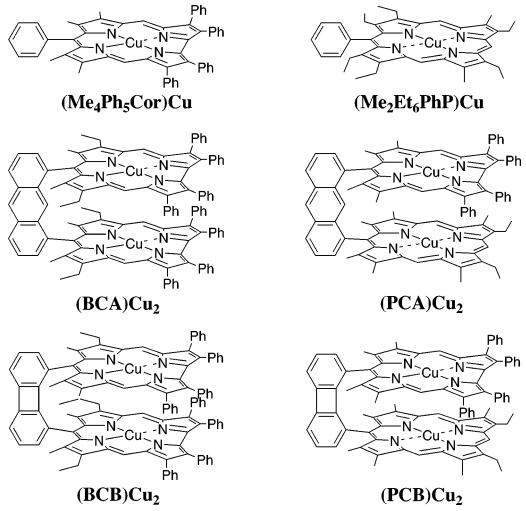

(Me_2Et_6PhP)Cu (Chart 1), are also presented, and the data are utilized as references to identify clearly the contribution of each counterpart in the overall properties of the bismacrocycles.

Experimental Section

Instrumentation. UV−vis spectra were recorded on a Varian Cary 1 spectrophotometer. Mass spectra were obtained on a Bruker ProFLEX III spectrometer in the matrix-assisted laser desorption ionization time-of-flight (MALDI-TOF) mode using dithranol as a matrix. Microanalyses were performed at the Université de Bourgogne on a Fisons EA 1108 CHNS instrument. ^{1}H NMR spectra were recorded on a Bruker DRX-500 AVANCE Fourier transform spectrometer at the "Centre de Spectrométrie Moléculaire de l'Université de Bourgogne"; chemical shifts are expressed in ppm relative to toluene-d_8 (2.09, 6.98, 7.00, and 7.09 ppm). The electron spin resonance (ESR) spectra were recorded at the X band (9.6 GHz) in solution on a Bruker ESP 300 spectrometer, from the "Centre de Spectrométrie Moléculaire de l'Université de Bourgogne", equipped with a liquid nitrogen cooling accessory. ESR spectra are referenced to 2,2-diphenyl-1-picrylhydrazyl (DPPH, $g = 2.0036$).

The magnetic susceptibility of the five compounds was measured over the temperature range 5−300 K at 0.5 and 5 T with a superconducting quantum interference device (SQUID) magnetometer SHE 700 and at 0.5, 1, 2.5, and 5 T with a SQUID magnetometer Quantum Design MPMS. The samples (5−26 mg) were contained in a kel-F bucket that had been independently calibrated at the same fields and temperatures. The data were corrected from diamagnetism using Pascal's constants.[52]

Cyclic voltammetry was carried out with an EG&G model 173 potentiostat. A three-electrode system was used and consisted of a glassy carbon or platinum disk working electrode, a platinum wire counter electrode and a saturated calomel reference electrode (SCE). The SCE electrode was separated from the bulk of the solution by a fritted-glass bridge of low porosity that contained the solvent/supporting electrolyte mixture. Half-wave potentials were calculated as $E_{1/2} = (E_{pa} + E_{pc})/2$ and are referenced to SCE.

UV−vis spectroelectrochemical experiments were performed with an optically transparent platinum thin-layer electrode of the type described in the literature.[53] Potentials were applied with an EG&G model 173 potentiostat. Time-resolved UV−vis spectra were recorded with a Hewlett-Packard model 8453 diode array rapid-scanning spectrophotometer.

X-ray Data Collection and Structure Determination Details for (BCB)Cu_2, (BCA)Cu_2, and (PCB)Cu_2. Single-crystals suitable for X-ray diffraction analysis were obtained from (BCB)Cu_2, (BCA)Cu_2, and (PCB)Cu_2, exhibiting prismatic-plate morphologies and dark-red colors. The dimensions of the selected specimens were $0.25 \times 0.12 \times 0.08$ mm^3 for (BCB)Cu_2, $0.30 \times 0.20 \times 0.04$ mm^3 for (BCA)Cu_2, and $0.25 \times 0.18 \times 0.05$ mm^3 for (PCB)Cu_2. Data were collected at low temperature ($T = 112$, 173, and 110 K for (BCB)Cu_2, (BCA)Cu_2, and (PCB)Cu_2, respectively) on two Nonius Kappa CCD diffractometers[54] using Mo Kα graphite monochromatic radiation ($\lambda = 0.71073$ Å) from a sealed tube. In the three crystal structure determinations, lattice parameters were obtained by a least-squares fit to the optimized setting angles of all reflections in the full θ-range data collection. Intensity data were recorded as φ scans for (BCA)Cu_2 and as φ and ω scans with κ offsets for (BCB)Cu_2 and (PCB)Cu_2, respectively. Data reductions were done using the DENZO software.[55] The structures were solved by direct methods using the SIR92 program.[56] Refinements were carried out by full-matrix least squares on F with $I > 3\sigma(I)$ data using the LSFM OpenMoleN program [57] for (BCA)Cu_2, and on F^2 with all data using the SHELXL97 program[58] for (BCB)Cu_2 and (PCB)Cu_2.

X-ray crystallographic files, in CIF format, for the structure determination of (BCB)Cu_2, (BCA)Cu_2, and (PCB)Cu_2 have been deposited at the CCDC and are available on request from the Director of the Cambridge Crystallographic Data Center, 12 Union Road, GB-Cambridge CN2 1EZ, U.K., on quoting the full journal citation.

Crystal Data for (BCB)Cu_2($C_{110}H_{82}N_8Cu_2 \cdot 3CDCl_3$). Experimental and crystal data of (BCB)Cu_2 are given in Table 1. Anisotropic thermal parameters were used for non-H atoms. Hydrogens and deuteriums were placed at calculated positions as riding atoms. They were refined with two different global isotropic thermal factors, corresponding to either H or D atoms. One of the three $CDCl_3$ solvent molecules belonging to the asymmetric unit was found to be disordered between two positions very close to each other. The corresponding sites occupation factors were refined, leading to the values 0.81(1)/0.19(1). The final agreement factors are $R(F) = 0.1011$ and $R_w(F^2) = 0.2368$ for $I > 2\sigma(I)$ data. At convergence, the maximum and minimum residual electron densities (1.25/−1.90 eÅ^{-3}) were found in the asymmetric unit region occupied by the disordered solvent molecule, indicating that its modeling was not accurately achieved.

Crystal Data for (BCA)Cu_2($C_{112}H_{84}N_8Cu_2 \cdot C_7H_8 \cdot 1.5H_2O$). Experimental and crystal data of (BCA)Cu_2 are given in Table 1. Anisotropic thermal parameters were used for non-H atoms except for the oxygens of the disordered water molecules (Ow), which were refined with an isotropic thermal factor. Hydrogens were placed at calculated positions as riding atoms, except those corresponding to the water molecules, which were not found. Their isotropic thermal parameters were fixed at $U_{iso}(H) = 1.3U_{equiv}(C)$

(52) Kahn, O. *Molecular Magnetism*; VCH: New York, 1993.
(53) Lin, X. Q.; Kadish, K. M. *Anal. Chem.* **1985**, *57*, 1498−1501.
(54) *COLLECT: Data Collection Software*; Nonius BV: Delft, The Netherlands, 1998.
(55) Otwinowski, Z.; Minor, W. In *Methods Enzymol.* **1997**, *276*, 307−326 (DENZO software).
(56) Sheldrick, G. M. *SHELXS97: Program for the Solution of Crystal Structures*; University of Göttingen: Göttingen, Germany, 1997.
(57) *OpenMoleN, I.S.S.*; Nonius BV: Delft, The Netherlands, 1997.
(58) Sheldrick, G. M. *SHELXL97: Program for the Refinement of Crystal Structures*; University of Göttingen: Göttingen, Germany, 1997.

Table 1. Selected Crystallographic Experimental Data

	(BCB)Cu_2	(BCA)Cu_2	(PCB)Cu_2
chemical formula	$C_{110}H_{82}N_8Cu_2{\cdot}3CDCl_3$	$C_{112}H_{84}N_8Cu_2{\cdot}C_7H_8{\cdot}1.5H_2O$	$C_{89}H_{71}N_8Cu_2{\cdot}CHCl_3$
formula weight	2001.02	1788.22	1498.99
temperature, K	112(2)	173(2)	110(2)
wavelength, Å	0.71073	0.71073	0.71073
crystal system	triclinic	monoclinic	monoclinic
space group	$P\bar{1}$	$P2_1/c$	$P2_1/n$
a, Å	10.2550(2)	16.0870(4)	16.7071(3)
b, Å	16.3890(3)	35.109(2)	10.6719(2)
c, Å	29.7910(8)	19.1390(8)	40.8555(8)
α, deg	74.792(1)	90	90
β, deg	81.681(1)	95.183(3)	100.870(1)
γ, deg	72.504(2)	90	90
volume, Å^3	4596.3(2)	10765(1)	7153.7(2)
Z	2	4	4
μ, mm^{-1}	0.782	0.446	0.762
crystal size, mm^3	0.25 × 0.12 × 0.08	0.30 × 0.20 × 0.04	0.25 × 0.18 × 0.05
collected reflections	28 293	46 974	28 418
unique reflections	20 205	12 733	11 613
R_{int}	0.085	0.087	0.045
θ_{max}, deg	28.9	24.1	27.4
refinement method	full-matrix least-squares on F^2	full-matrix least-squares on F	full-matrix least-squares on F^2
data/parameters	20 205/1236	8804/1178	11 613/944
goodness-of-fit on F^2	1.022	1.124	1.072
R1/wR2[a] ($I > 2\sigma(I)$)[b]	0.101/0.237	0.094/0.104	0.067/0.135
$\Delta\rho_{max}/\Delta\rho_{min}$, eÅ^{-3}	1.25/−1.90	1.15/−0.25	0.78/−0.71

[a] $R1 = \sum||F_o| - |F_c||/\sum|F_o|$ and $wR2 = [\sum[w(F_o^2 - F_c^2)^2]/\sum[w(F_o^2)^2]]^{1/2}$. [b] $I > 3\sigma(I)$ for (BCA)Cu_2.

(C = carbon atom bonded to H). One water molecule belonging to the asymmetric unit was found to be disordered among three positions, showing Ow···Ow distances of 2.30, 2.59, and 3.39 Å. The corresponding Ow sites occupation factors (sof's) were fixed at $^1/_3$ each. A second water molecule was found in the asymmetric unit partially occupying a unique site and the sof of the Ow atom was fixed at $^1/_2$. The final agreement factors are $R(F) = 0.094$ and $R_w(F^2) = 0.104$ for $I > 3\sigma(I)$ data. The maximum and minimum residual electron densities are 1.15/−0.25 eÅ^{-3}.

Crystal Data for (PCB)Cu_2($C_{89}H_{71}N_8Cu_2{\cdot}CHCl_3$). Experimental and crystal data of (PCB)Cu_2 are given in Table 1. Anisotropic thermal parameters were used for non-H atoms. Hydrogens were placed at calculated positions as riding atoms. They were refined with a global isotropic thermal parameters. The final agreement factors are $R(F) = 0.0668$ and $R_w(F^2) = 0.1350$ for $I > 2\sigma(I)$ data. The maximum and minimum residual electron densities are 0.78/−0.71 eÅ^{-3}.

Chemicals and Reagents. Absolute dichloromethane (CH_2Cl_2) and pyridine (py) were obtained from Fluka Chemical Co. and used as received. Benzonitrile (PhCN) was purchased from Aldrich Chemical Co. and distilled over P_2O_5 under vacuum prior to use. Neutral alumina (Merck; usually grade III, i.e., deactivated with 6% water) and silica gel (Merck; 70−120 mm) were used for column chromatography. Analytical thin-layer chromatography was performed using Merck 60 F254 silica gel (precoated sheets, 0.2 mm thick). Reactions were monitored by thin-layer chromatography and UV−vis spectroscopy. Tetra-*n*-butylammonium perchlorate (TBAP, Fluka Chemical Co.) was twice recrystallized from absolute ethanol and dried in a vacuum oven at 40 °C for a week prior to use.

Starting Compounds. The following free-base compounds were synthesized according to previously described procedures: 1,8-bis-(7,13-diethyl-8,12-dimethyl-2,3,17,18-tetraphenylcorrol-10-yl)-anthracene (BCA)H_6,[42,45,47] 1,8-bis-(7,13-diethyl-8,12-dimethyl-2,3,17,18-tetraphenylcorrol-10-yl)biphenylene (BCB)H_6,[42,45,47] 1-(13,-17-diethyl-2,3,7,8,12,13,18-hexamethylporphyrin-5-yl)-8-(7,8,-12,13-tetramethyl-2,3,17,18-tetraphenylcorrol-10-yl)anthracene (PCA)H_5,[41,44−46] 1-(13,17-diethyl-2,3,7,8,12,18-hexamethylporphyrin-5-yl)-8-(2,3,17,18-tetraphenyl-7,8,12,13-tetramethylcorrol-10-yl)biphenylene, (PCB)H_5,[41,44,45] 2,3,7,8,12,18-hexaethyl-13,17-dimethyl-5-phenylporphyrin (Me_2Et_6PhP)H_2,[41,42] and 7,8,12,13-tetramethyl-2,3,10,17,18-pentaphenylcorrole (Me_4Ph_5Cor)H_3.[41−43]

Copper Complexes. The molecular schemes of the copper derivatives are shown in Chart 1.

(BCA)Cu_2, 1,8-Bis-[copper-7,13-diethyl-8,12-dimethyl-2,3,-17,18-tetraphenylcorrol-10-yl]anthracene. A solution of 400 mg (0.26 mmol) of the biscorrole dyad (BCA)H_6 and 300 mg (2.23 mmol) of copper(II) dichloride in 40 mL of pyridine was stirred under argon at 40 °C for 2 h, the metalation reaction being monitored by UV−vis spectroscopy. The solvent was then evaporated under vacuum, and the crude solid thus obtained was dissolved in dichloromethane. The organic solution was washed four times with water to remove any trace of copper salt and then dried over magnesium sulfate. Chromatography on basic alumina using CH_2Cl_2/heptane (60/40) afforded the title product (m = 0.100 g; 23%) which corresponds to the first eluted compound. MS (MALDI-TOF): m/z = 1668.99 $[M]^{+\bullet}$, 1669.04 calcd for $C_{112}H_{84}N_8Cu_2$. UV−vis (CH_2Cl_2), λ_{max}, nm ($\epsilon \times 10^{-3}$, M^{-1} cm^{-1}) = 410 (130), 570 (25.1). Anal. Calcd for $C_{112}H_{84}N_8Cu_2$: C, 80.60; H, 5.07; N, 6.71. Found: C, 80.71; H, 5.61; N, 6.37.

(BCB)Cu_2, 1,8-Bis-[copper-7,13-diethyl-8,12-dimethyl-2,3,17,-18-tetraphenylcorrol-10-yl]biphenylene. This compound was prepared in 17% yield (65 mg) as described for (BCA)Cu_2, starting from (BCB)H_6 (350 mg, 0.23 mmol). MS (MALDI-TOF): m/z = 1642.70 $[M]^{+\bullet}$, 1643.00 calcd for $C_{110}H_{82}N_8Cu_2$. UV−vis (CH_2Cl_2), λ_{max}, nm ($\epsilon \times 10^{-3}$, M^{-1} cm^{-1}): 404 (118), 570 (20.8). Anal. Calcd for $C_{110}H_{82}N_8Cu_2$: C, 80.41; H, 5.03; N, 6.82. Found: C, 80.23; H, 5.36; N, 6.48.

(PCA)Cu_2, 1-(Copper-2,3,7,8,12,18-hexamethyl-13,17-diethylporphyrin-5-yl)-8-(copper-2,3,17,18-tetraphenyl-7,8,12,13-tetramethylcorrol-10-yl)anthracene. This compound was prepared in 38% yield (150 mg) in pyridine under reflux as described for (BCA)Cu_2, starting from (PCA)H_5 (350 mg, 0.27 mmol). MS (MALDI-TOF): m/z = 1405.19 $[M]^{+\bullet}$, 1405.73 calcd for $C_{91}H_{73}N_8Cu_2$. UV−vis (CH_2Cl_2), λ_{max}, nm ($\epsilon \times 10^{-3}$, M^{-1} cm^{-1}): 403 (198), 533 (16.9), 566 (20.7). Anal. Calcd for

Scheme 1

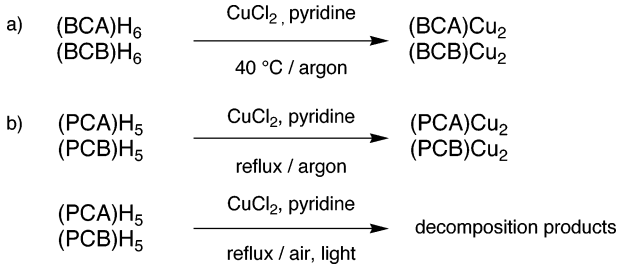

$C_{91}H_{73}N_8Cu_2$: C, 77.75; H, 5.23; N, 7.97. Found: C, 77.81; H, 5.71; N, 7.54.

(PCB)Cu_2, 1-(Copper-2,3,7,8,12,18-hexamethyl-13,17-diethylporphyrin-5-yl)-8-(copper-2,3,17,18-tetraphenyl-7,8,12,13-tetramethylcorrol-10-yl)biphenylene. This compound was prepared in 27% yield (45 mg) in pyridine under reflux as described for (BCA)Cu_2, starting from (PCB)H_5 (150 mg, 0.12 mmol). MS (MALDI-TOF): m/z = 1379.27 $[M]^{+\bullet}$, 1379.69 calcd for $C_{89}H_{71}N_8Cu_2$. UV−vis (CH_2Cl_2), λ_{max}, nm ($\epsilon \times 10^{-3}$, M^{-1} cm^{-1}): 397 (247), 528 (16.4), 563 (21.3). Anal. Calcd for $C_{89}H_{71}N_8Cu_2$: C, 77.48; H, 5.19; N, 8.12. Found: C, 77.67; H, 4.88; N, 7.86.

(Me_2Et_6PhP)Cu, Copper-2,3,7,8,12,18-hexaethyl-13,17-dimethyl-5-phenylporphyrin. This compound was prepared in 38% yield (42 mg), as described for (BCA)Cu_2, starting from (Me_2Et_6PhP)H_2 (100 mg, 0.17 mmol). MS (MALDI-TOF): m/z = 644.11 $[M]^{+\bullet}$, 644.36 calcd for $C_{40}H_{44}N_4Cu$. UV−vis (CH_2Cl_2), λ_{max}, nm ($\epsilon \times 10^{-3}$, M^{-1} cm^{-1}): 403 (318), 529 (15.0), 565 (20.0). Anal. Calcd for $C_{40}H_{44}N_4Cu$: C, 74.56; H, 6.88; N, 8.69. Found: C, 74.95; H, 6.39; N, 8.38.

(Me_4Ph_5Cor)Cu, Copper-7,8,12,13-tetramethyl-2,3,10,17,18-pentaphenylcorrole. This compound was prepared in 37% yield (48 mg), as described for (BCA)Cu_2, starting from (Me_4Ph_5Cor)H_3 (120 mg, 0.16 mmol). MS (MALDI-TOF): m/z = 795.11 $[M]^{+\bullet}$, 795.46 calcd for $C_{53}H_{39}N_4Cu$. UV−vis (CH_2Cl_2), λ_{max}, nm (ϵ x 10^{-3}, M^{-1} cm^{-1}): 410 (101), 569 (17.3). Anal. Calcd for $C_{53}H_{39}N_4Cu$: C, 80.03; H, 4.94; N, 7.04. Found: C, 79.67; H, 4.76; N, 6.88.

Results and Discussion

Synthesis and Physicochemical Characterization. The complexes (BCA)Cu_2 and (BCB)Cu_2 were synthesized by heating the corresponding free-base ligand, (BCA)H_6 or (BCB)H_6, with excess $CuCl_2$ in pyridine at 40 °C under argon (Scheme 1a).[59] The Soret band of (BCA)Cu_2 is located at 410 nm, and a Q band is observed at 570 nm as compared to 410 and 569 nm for the monocorrole derivative, (Me_4Ph_5Cor)Cu, in CH_2Cl_2. The UV−vis spectra of (BCA)Cu_2 and (BCB)Cu_2 display an intense Soret band indicating that the aromatic system of both bismacrocycles remains unaltered after metalation. Conversely, it should be noted that, under the same reaction conditions, nickel bisoxocorroles are formed by metalation of the same biscorroles with a nickel salt.[45]

Mass spectral analysis confirms the structures of (BCA)Cu_2 and (BCB)Cu_2 by exhibiting a single ion pattern at m/z = 1669 for the anthracenyl derivative and at m/z = 1643 for the biphenylenyl derivative. No trace of a bisoxocorrole nor of any monometallic derivative could be observed by ^{1}H NMR or mass spectrometry.[45]

The copper complexes of the corresponding porphyrin−corrole, (PCA)H_5 and (PCB)H_5, were synthesized by heating the free-base ligand with excess copper(II) chloride in refluxing pyridine under argon as described in Scheme 1b. When the metalation was carried out under air and in the presence of light, a significant decomposition of the complex was observed. Attempts to isolate the decomposition products were unsuccessful. Conversely, no decomposition occurs when the bismacrocycle is metalated under an inert argon atmosphere, and the copper complexes are obtained in 38 and 27% yields for (PCA)Cu_2 and (PCB)Cu_2, respectively.

The electronic absorption spectra of (PCA)Cu_2 in CH_2Cl_2 (λ_{max} = 403 (Soret band), 533, 566 nm) and (PCB)Cu_2 in CH_2Cl_2 (λ_{max} = 397 (Soret band), 528, 563 nm) show a slightly blue-shifted Soret and Q band as compared to the biscorrole counterparts (BCA)Cu_2 (λ_{max} = 410 (Soret band), 570 nm) and (BCB)Cu_2 (λ_{max} = 404 (Soret band), 569 nm, see Experimental Section), the wavelength differences between the Soret band of the porphyrin−corrole and its biscorrole analogue being equal to 7 nm, independent of the spacer type (A or B). This slight blue shift in λ_{max} indicates a larger ring current for the porphyrin chromophore than for the corrole macrocycle. As already observed in the case of bimetallic Pacman bisporphyrins,[50,60,61] the biphenylenyl complex (PCB)Cu_2 exhibits an electronic absorption spectrum with a more blue-shifted Soret band than the anthracenyl (PCA)Cu_2 analogue. This feature is in good agreement with the cofacial geometry of the porphyrin and corrole rings and is due to a larger $\pi-\pi$ interaction in the case of the PCB derivative that has a smaller interplanar distance between the two macrocycles (see following X-ray crystallography section).[41,42]

The mass spectral data of the porphyrin−corrole copper complexes are given in the Experimental Section. The molecular peak of the biscopper complex, (PCA)Cu_2 or (PCB)Cu_2, was observed at m/z = 1405 and 1379 for (PCA)Cu_2 and (PCB)Cu_2, respectively, and the data are in perfect agreement with the expected molecular formula. No additional major peaks are seen.

ESR and ^{1}H NMR Characterizations. Further indications of the nature of the biscopper complexes are provided by ESR and ^{1}H NMR spectroscopies (in toluene solutions) and also by the magnetic susceptibility determination on powdered samples in the 5−300 K temperature range as discussed in the next section.

The ESR spectrum of the porphyrin−corrole derivative, (PCA)Cu_2, in frozen toluene solution at 100 K (see Supporting Information) is centered at $g_{||}$ = 2.21 and $g_{\perp}$ = 2.05 and shows a four-line hyperfine splitting due to the Cu nucleus (I = $^3/_2$, $a_{||}^{Cu}$ = 203 G) as well as a nine-line superhyperfine splitting due to the four porphyrin nitrogens, which is clearly observed in the high-field part of the

(59) Will, S.; Lex, J.; Vogel, E.; Schmickler, H.; Gisselbrecht, J.-P.; Haubtmann, C.; Bernard, M.; Gross, M. *Angew. Chem., Int. Ed. Engl.* **1997**, *36*, 357−361.

(60) Bolze, F.; Gros, C. P.; Drouin, M.; Espinosa, E.; Harvey, P. D.; Guilard, R. *J. Organomet. Chem.* **2002**, 89−97.

(61) Bolze, F.; Drouin, M.; Harvey, P. D.; Gros, C. P.; Guilard, R. *J. Porphyrins Phthalocyanines* **2003**, *7*, 474−483.

spectrum ($a_{\perp}^{N} = 17.7$ G). No forbidden transition is observed in the half-field part of the ESR spectrum, indicating the absence of any Cu−Cu interaction[62] and the presence of a "pure" Cu(II) porphyrin and diamagnetic Cu(III) corrole species as expected. The shape of the ESR spectrum of $(PCB)Cu_2$ is relatively close to that of $(PCA)Cu_2$. The signal of $(PCB)Cu_2$ is centered at $g_{\parallel} = 2.18$ and $g_{\perp} = 2.05$ and exhibits the same four-line hyperfine splitting due to the Cu nucleus ($I = {}^3/_2$, $a_{\parallel}^{Cu} = 208$ G) and the nine-line superhyperfine splitting from the four porphyrin nitrogens at high field ($a_{\perp}^{N} = 17.2$ G). Those data clearly indicate the presence of one ESR-active Cu(II) species in the cofacial porphyrin−corrole system, and this would be in the porphyrin macrocycle. The ESR spectra of $(PCA)Cu_2$ and $(PCB)Cu_2$ do not significantly differ from those of Cu(II) porphyrins and other N-donor ligand complexes for which a broad resonance signal at $g = 2.2-2.3$ is typical.[62] However, in the case of $(PCB)Cu_2$, extra lines appear at 3117 and 3600 G that could indicate the presence of a small amount of a radical (i.e., a Cu(II)$^{\bullet}$ corrole species). As for $(PCA)Cu_2$, no forbidden half-field transition was observed, indicating the absence of any Cu−Cu interaction.

The ESR spectrum of $(BCA)Cu_2$ clearly indicates the presence of a Cu(II)$^{\bullet}$ corrole species ($g_{\parallel} = 2.18$, $a_{\parallel}^{Cu} = 201$ G; $g_{\perp} = 2.08$, $a_{\perp}^{N} = 17.0$ G), the two Cu(II)$^{\bullet}$ corrole macrocycles being in the same environment, which is not the case for $(BCB)Cu_2$. Two types of resonances for the Cu(II)$^{\bullet}$ corrole species are observed in the ESR spectrum of $(BCB)Cu_2$. However, the overlap of the signals and their very low intensity do not allow assignment of the ESR resonances, and the presence of the diamagnetic Cu(III) corrole complex has to be considered as the major contribution.

The $(Me_4Ph_5Cor)Cu$ complex is also ESR-active, but the signal-to-noise ratio, as observed for biscorrole derivatives, is very weak compared to that of the monocopper porphyrin Cu(II) complexes such as $(Me_2Et_6PhP)Cu$ or (TPP)Cu. This result indicates that the amount of Cu(II)$^{\bullet}$ corrole is small compared to the amount of the major Cu(III) complex and that the presence of a non-ESR active species such as a Cu(III) derivative has to be considered mainly at low temperature. The ESR spectra for each derivative were also recorded at variable temperatures up to 373 K. The isotropic spectra give no further indication of an increasing ratio of paramagnetic species at higher temperature.

The influence of temperature on the distribution of species in each oxidation state is more evident from the variable-temperature NMR studies (in toluene solution). The shape of the ^{1}H NMR spectrum is in agreement with the presence of a dominant diamagnetic species, but heating of the sample in the NMR magnet from 183 to 360 K causes line shifts and line broadening. This is shown in Figure 1 in the case of the $(BCB)Cu_2$ derivative. Line broadening and a chemical shift temperature dependence are not observed for each resonance. This behavior can be understood as an overlapping

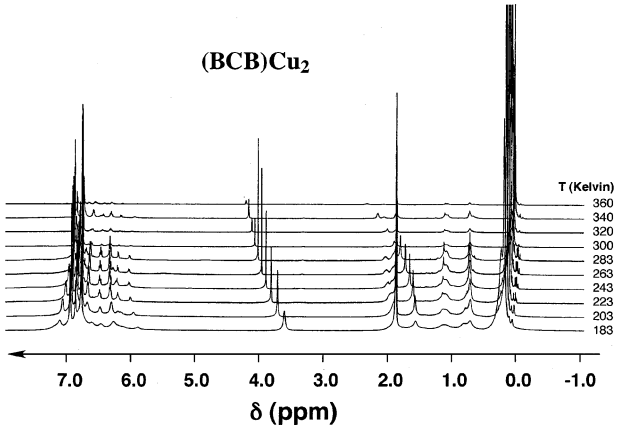

Figure 1. ^{1}H NMR spectra (500 MHz, toluene-d_8, δ) of $(BCB)Cu_2$ recorded at different temperatures.

of two types of ^{1}H NMR spectra (i.e., a diamagnetic spectrum and a paramagnetic spectrum, the first one being attributable to the Cu(III) derivative and the second one, to a Cu(II)$^{\bullet}$ species). The strongest temperature effect is clearly observed for the alkyl resonances at around 4.0 ppm with a low-field chemical shift change of +0.7 ppm between 183 and 360 K for the $(BCB)Cu_2$ complex (see Figure 1). Also the significant signal broadening above 320 K indicates a stronger paramagnetism when increasing the temperature. These ^{1}H NMR results are in good agreement with the presence of unpaired spin density on some proton sites. No clear-cut assignment is possible due to the overlapping resonances and poorly resolved signals.

The observed shifts are reversible upon cooling the sample back to 183 K. A similar trend is also observed in the case of $(BCA)Cu_2$ as well as in the case of the monocorrole species. These results suggest a developing paramagnetism upon raising the temperature. A similar result was earlier observed in the case of copper octafluorocorroles,[17] copper triphenylcorroles,[39] and copper β-octaalkylcorroles.[59] In all cases, the authors attributed their observations to a thermally accessible copper(II) π-cation radical excited state, the diamagnetic Cu(III) ground state being the dominant species whatever the temperature.

In summary, the variable-temperature ESR and NMR experiments carried out with the four cofacial biscopper derivatives show the presence of an equilibrium between (Cor)Cu(II)$^{\bullet}$ and (Cor)Cu(III), the (Cor)Cu(III) species being the major one, as clearly evidenced by the NMR studies (i.e., the diamagnetic NMR spectra).

Magnetic Properties of the Porphyrin−Corrole and Biscorrole Derivatives. A similar trend can be seen from the magnetic susceptibility experiments in the solid state. The magnetic susceptibility of all compounds has been investigated in the temperature range 5−300 K at four fields from 0.5 to 5 T. It is illustrated in Figure 2 as the temperature dependence of the product of the molar magnetic susceptibility (χ_M) by temperature. All compounds exhibit the same behavior characterized by a constant value of $\chi_M T$ from room temperature down to ca. 10 K. This excludes the presence of a noticeable magnetic exchange coupling between the two copper centers in the biscorrole and porphy-

(62) Eaton, S. S.; Eaton, G. R.; Chang, C. K. *J. Am. Chem. Soc.* **1985**, *107*, 3177−3184.

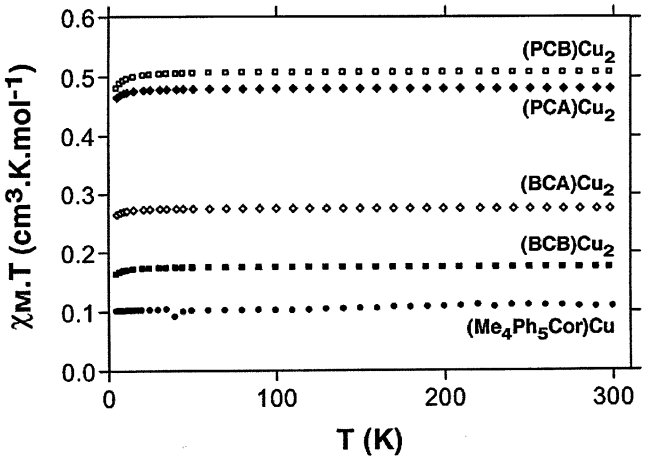

Figure 2. Temperature dependence of $\chi_M T$ for $(Me_4Ph_5Cor)Cu$, $(BCB)Cu_2$, $(BCA)Cu_2$, $(PCA)Cu_2$, and $(PCB)Cu_2$. Data collected in the temperature range 5−300 K.

rin−corrole derivatives. In addition, a small decrease is observed at low temperatures ($T < 10$ K) that can be attributed to intermolecular interactions in the solid. The monocorrole complex presents a constant $\chi_M T$ at 0.1 cm^3 K mol^{-1} over the whole temperature range, which illustrates the occurrence of a small paramagnetic contribution. The two biscorroles exhibit a plateau at $\chi_M T = 0.17$ and 0.27 cm^3 K mol^{-1} for the BCB and BCA complexes, respectively. Consistent with the dinuclear nature of the compounds, these values are roughly double that of the monocorrole derivative. Nevertheless, they show a significant dependency on the nature of the spacer for the biscorrole complexes, which may be ascribed to their different abilities to mediate $\pi-\pi$ interactions as revealed in ESR and electrochemistry (see below). In addition, the two porphyrin−corroles exhibit very similar behavior with $\chi_M T$ values of 0.49(2) cm^3 K mol^{-1}. The latter value can be explained by considering that it corresponds to the addition of the copper(II) porphyrin contribution to that of the copper corrole. Indeed, from the *g* values measured by ESR spectroscopy one can estimate that the copper porphyrin will contribute to a value of 0.41 cm^3 K mol^{-1} for the product $\chi_M T$. A contribution of 0.08(2) cm^3 K mol^{-1} from the copper corrole moiety to the product $\chi_M T$ can therefore be estimated, consistent with that measured for the monocorrole. In this case, the nature of the spacer has no effect because the copper(II)−porphyrin moiety has no radical character.

The weak paramagnetism exhibited by the copper corrole moiety is not consistent with a solely Cu(III) description, which would be diamagnetic. Similarly, it is also not consistent with a $(Cor)Cu(II)^{\bullet}$ formulation because this species would exhibit either a spin of $S = 1$ (strong ferromagnetic coupling), a spin of $S = 0$ (strong antiferromagnetic coupling), or a temperature-dependent spin (intermediate magnetic coupling). Thus, the results of magnetic measurements are in accordance with those of the ESR and NMR experiments. The monocorrole copper, biscorrole biscopper, and porphyrin−corrole biscopper derivatives have to be considered as an equilibrium between compounds with a major Cu(III) metal center and a minor Cu(II) radical one,

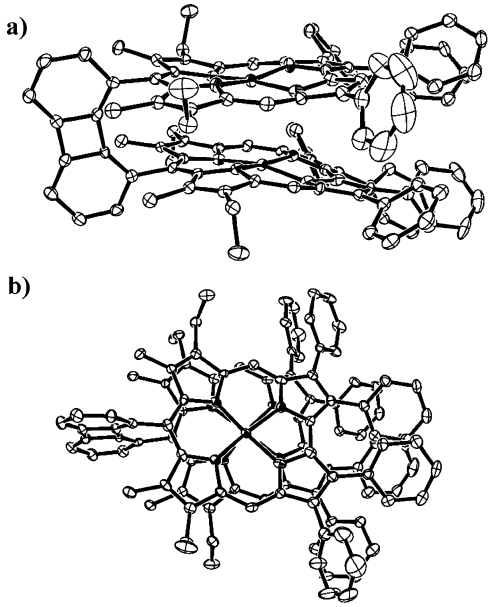

Figure 3. ORTEP view of the $(BCB)Cu_2$ dimer: (a) lateral and (b) apical views. Hydrogen atoms are omitted for clarity. Thermal ellipsoids are drawn at the 50% probability level.

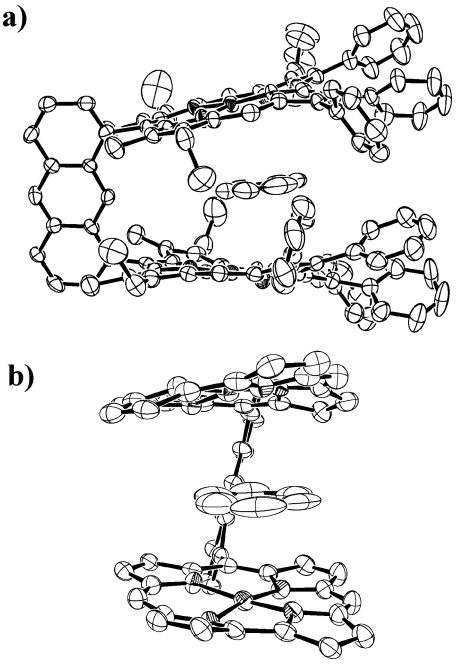

Figure 4. ORTEP view of the $(BCA)Cu_2$ dimer: (a) lateral and (b) side views. Hydrogen atoms are omitted for clarity. Thermal ellipsoids are drawn at the 50% probability level.

independent of temperature. No significant temperature dependence is observed in the solid state.

Description of the $(BCB)Cu_2$, $(BCA)Cu_2$, and $(PCB)Cu_2$ Molecular Structures. Lateral and apical views of the $(BCB)Cu_2$, $(BCA)Cu_2$, and $(PCB)Cu_2$ molecular structures are given in Figures 3−5, respectively. Table 1 gives crystal data and some experimental and refinement details for the three crystal structures. Selected Cu−N bond distances and geometrical parameters describing the molecular conformations of the reported complexes are summarized in Tables 2 and 3. Along with these data are given

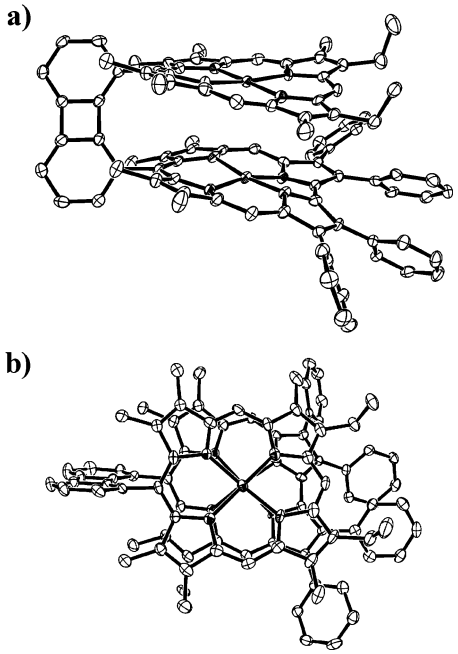

Figure 5. ORTEP view of the (PCB)Cu_2 dimer: (a) lateral and (b) apical views. Hydrogen atoms are omitted for clarity. Thermal ellipsoids are drawn at the 50% probability level.

the corresponding values for other face-to-face homobimetallic copper complexes ((DPB)Cu_2,[63] (BC*m*S)Cu_2,[64] and (DPX)Cu_2[65]) as well as the related nickel derivatives ((BOCA)Ni_2,[45] (DPA)Ni_2,[63] and (DPX)Ni_2[65]) where DPB represents diporphyrin biphenylenyl, BC*m*S is bis*meso*corrole dibenzothiophene, DPX is diporphyrin 9,9-dimethylxanthene, BOCA is bisoxocorrole anthracenyl, and DPA represents diporphyrin anthracenyl; see Chart 2. Data for two monocorrole copper complexes ((TPC*m*)Cu,[39] (TETMC)Cu[59]) are also listed in Tables 2 and 3 where TPC*m* represents *meso*-triphenylcorrole and TETMC is tetraethyltetramethylcorrole.

Macrocycle Conformation. The macrocycles are slightly distorted in the three reported complexes, the mean C deviations from their two least-squares mean planes (MDMP, see Table 2) being 0.13/0.15 for (BCB)Cu_2, 0.12/0.25 for (BCA)Cu_2, and 0.23/0.23(3) Å for (PCB)Cu_2. Both corrole rings are ruffled in (BCB)Cu_2, as indicated by the displacements of the meso carbon atoms (C-meso) above and below the macrocyclic mean planes. Thus, for this complex, the C-meso atoms anchored to the spacer are 0.12 and 0.18 Å below their respective planes, although the other two are 0.09/0.18 and 0.12/0.19 Å above each plane. Although similar features are found in the ruffled corrole moiety of (PCA)Cu_2 (showing the respective C-meso atoms at 0.15 Å below and at 0.02/0.21 Å above the macrocycle mean plane), three of them are found above the corresponding plane (at 0.02, 0.02, and 0.07 Å) in its porphyrin moiety, and the fourth one is observed below the plane (at 0.02 Å). In that case, where the four C-meso atoms are close to the least-squares mean plane, the relative position of the nitrogen atoms (lying above and below the plane at 0.07/0.16 Å and at 0.01/0.02 Å, by pairs of opposite pyrrole groups, respectively) indicates an approximate saddle conformation. In (BCA)Cu_2, the corrole rings are slightly wave-shaped, exhibiting two adjacent C-meso atoms at the same side of the least-squares mean plane (at 0.02/0.03 Å and 0.03/0.06 Å, for each macrocycle) and a third one at the other side of the calculated plane (at 0.04 and 0.17 Å, for the corresponding macrocycles). The macrocyclic rings of (DPB)Cu_2 and (DPA)Ni_2 are saddle-shaped, although for (DPX)Cu_2 and (DPX)Ni_2 they are ruffle-shaped and in (BOCA)Ni_2 they are a mixture of irregular saddle, ruffle, and doming distortions. Comparing these face-to-face complexes, the corrole, and porphyrin rings show a large spread of distortions between the four commonly identified conformations, namely, saddle, wave, ruffle, and dome. Obviously, ring conformations are the result of several kinds of interactions, including coordination bonds, steric repulsions between substituents, packing forces, and the eventual macrocyclic $\pi-\pi$ and metal−metal interactions. As expected, because of the mixture of all of these contributions, there is no direct evidence of any correlation between the observed ring conformations and the metals, macrocycles, or aromatic spacers. Thus, for instance, even if (DPX)Zn_2, (DPX)Cu_2, and (DPX)Ni_2 have the same two porphyrin macrocycles and the same identical aromatic spacers, the (DPX)Zn_2 derivatives show for both porphyrin macrocycles a wave conformation, although (DPX)Cu_2 and (DPX)Ni_2 both exhibit ruffle conformations.[65]

Aromatic Spacers. Although the biphenylenyl spacer is almost planar in (PCB)Cu_2 and slightly distorted in (BCB)Cu_2 (the largest and the mean deviations from their respective mean planes being 0.05 and 0.03 Å, and 0.09 and 0.06 Å, respectively), the anthracenyl spacer exhibits a more significant distortion in (BCA)Cu_2 (the corresponding deviations being 0.13 and 0.07 Å). Throughout the series (PCB)Cu_2, (BCB)Cu_2, and (BCA)Cu_2, the observed deformations increase and lead to a concomitant increasing of the torsion angle between the $C_{meso,1}$, $C_{anch,1}$, $C_{anch,2}$, and $C_{meso,2}$ atoms, reflecting the twisted degree of the spacer (see Figure 6). The angle values are 5.0, 11.2, and 20.4° for (PCB)Cu_2, (BCB)Cu_2, and (BCA)Cu_2, respectively. This deformation correlates with the relative position of the macrocycles in each complex, going from a closely eclipsed conformation for (PCB)Cu_2 to a twisted conformation for (BCA)Cu_2; the average values of the four smallest torsion angles $N_{1j}-M_1-M_2-N_{2k}$ with $j, k = 1$ to 4 are 7.0, 7.9, and 17.6°, for (PCB)Cu_2, (BCB)Cu_2, and (BCA)Cu_2, respectively.

Bond Coordination Geometries. In (BCB)Cu_2, (BCA)Cu_2, and (PCB)Cu_2, the copper atoms are tetracoordinated by the four pyrrole nitrogens. Although the Cu_1-N_{pyr} bond coordination distances corresponding to the corrole ligands range from 1.89 to 1.92 Å (see Table 3), they are roughly 0.1 Å longer in the porphyrin moiety of (PCB)Cu_2, ranging from 1.99 to 2.01 Å. Similar geometries to those found in the porphyrin moiety of (PCB)Cu_2 are found for the corresponding coordination distances observed in the bisporphyrin complexes (DPB)Cu_2 and (DPX)Cu_2

(63) Fillers, J. P.; Ravichandran, K. G.; Abdalmuhdi, I.; Tulinsky, A.; Chang, C. K. *J. Am. Chem. Soc.* **1986**, *108*, 417−424.
(64) Pacholska, E.; Espinosa, E.; Guilard, R. *J. Chem. Soc., Dalton Trans.* **2004**, in press.
(65) Chang, C. J.; Deng, Y.; Heyduc, A. F.; Chang, C. K.; Nocera, D. J. *Inorg. Chem.* **2000**, *39*, 959−966.

Table 2. Selected Geometrical Parameters Derived from the Molecular Structures of $(BCB)Cu_2$, $(BCA)Cu_2$, $(PCB)Cu_2$, and Other Related Complexes

	d(Ct−Ct) (Å)	*d*(M−M) (Å)	Δd_2[a] (Å)	MDMP (Å)	MPS (Å)	M−LSMP (Å)	θ (deg)	α (deg)	*L* (Å)	*d*(a−b) (Å)	*d*(c−d) (Å)	Δd_1[b] (Å)	ref[d]
$(BCB)Cu_2$	4.13	4.02	−0.11	0.13/0.15	3.65	0.05/0.16	9.2	29.3	2.02	3.79	3.78	−0.01	*c*
$(BCA)Cu_2$	6.34	6.35	0.01	0.12/0.25	6.13	0.10/0.11	18.3	9.3	1.02	4.98	5.26	0.28	*c*
$(PCB)Cu_2$	3.73	3.63	−0.10	0.23/0.23	3.48	0.12/0.10	5.3	23.5	1.49	3.79	3.79	0.00	*c*
$(DPB)Cu_2$	3.86	3.81	−0.05	0.23/0.23	3.50	0.02/0.09	4.4	25.0	1.63	3.80	3.80	0.00	63
$(BC^mS)Cu_2$	7.66	7.68	0.02	0.18/0.19	5.91	0.03/0.14	5.2	39.5	4.87	5.25	6.27	1.02	64
$(DPX)Cu_2$	3.98	3.91	−0.07	0.12/0.15	3.60	0.05/0.10	4.6	25.3	1.74	4.59	4.32	−0.27	65
$[(TETMC)Cu]_2$	4.80	4.72	−0.08	0.07/0.08	3.42	0.05/0.03	0.5	45.1	3.40				59
$(DPX)Ni_2$	4.70	4.69	−0.01	0.14/0.29	3.60	0.00/0.01	2.6	40.0	3.02	4.66	4.47	−0.19	65
$(BOCA)Ni_2$	4.71	4.68	−0.03	0.17/0.22	4.29	0.05/0.04	7.8	24.0	1.91	4.93	4.89	−0.04	45
$(DPA)Ni_2$	4.59	4.57	−0.02	0.39/0.43	3.87	0.05/0.02	3.9	32.5	2.47	4.96	4.93	−0.03	63

[a] $\Delta d_2 = d(M-M) - d(Ct-Ct)$. [b] $\Delta d_1 = d(c-d) - d(a-b)$. [c] This work. [d] To compare homogeneous quantities, we recalculated selected geometrical parameters from the literature using the same definitions as indicated in Figure 6.

Table 3. Selected Bond Lengths and Distances from the Least-Squares Mean Plane (LSMP) to the Coordinated Metal Derived from the Molecular Structures of $(BCA)Cu_2$, $(BCB)Cu_2$, $(PCB)Cu_2$, and Other Related Complexes

	$(BCA)Cu_2$	$(BCB)Cu_2$	$(PCB)Cu_2$	$(DPB)Cu_2$[63,a]	$(BC^mS)Cu_2$[64]	$(DPX)Cu_2$[65]	$(TPC^m)Cu$[39]	(TETMC)Cu[59,b]
Cu1−N (C/P)[c]	1.899 (8)	1.887 (5)	1.897 (4)	2.002	1.892 (6)	2.008(9)	1.891 (4)	1.868 (5)
	1.893 (9)	1.894 (5)	1.904 (4)	1.991	1.895 (6)	2.011(9)	1.892 (4)	1.872 (6)
	1.903 (9)	1.916 (4)	1.909 (4)	1.996	1.883 (6)	2.001(9)	1.893 (4)	1.885 (5)
	1.917 (9)	1.916 (4)	1.913 (4)	1.997	1.898 (6)	2.016(9)	1.894 (4)	1.896 (5)
Cu2−N (C/P)[c]	1.898 (9)	1.894 (5)	1.993 (4)	1.993	1.897 (5)	1.980(10)		1.867 (6)
	1.900 (10)	1.897 (5)	2.004 (4)	1.994	1.889 (6)	2.013(9)		1.879 (6)
	1.911 (9)	1.901 (5)	2.007 (4)	1.997	1.894 (6)	1.992(9)		1.880 (6)
	1.911 (9)	1.906 (5)	2.008 (4)	2.002	1.904 (6)	1.995(9)		1.889 (6)

[a] Estimated standard deviations from average bond lengths are 0.002 and 0.004 Å for shorter and longer geometries, respectively. [b] Two crystallographically independent copper corrole molecules are found in the asymmetric unit. [c] The symbol "C/P" means corrole (C) or porphyrin (P) macrocycle. TPC^m = meso-triphenylcorrole, TETMC = tetraethyltetramethylcorrole.

Chart 2

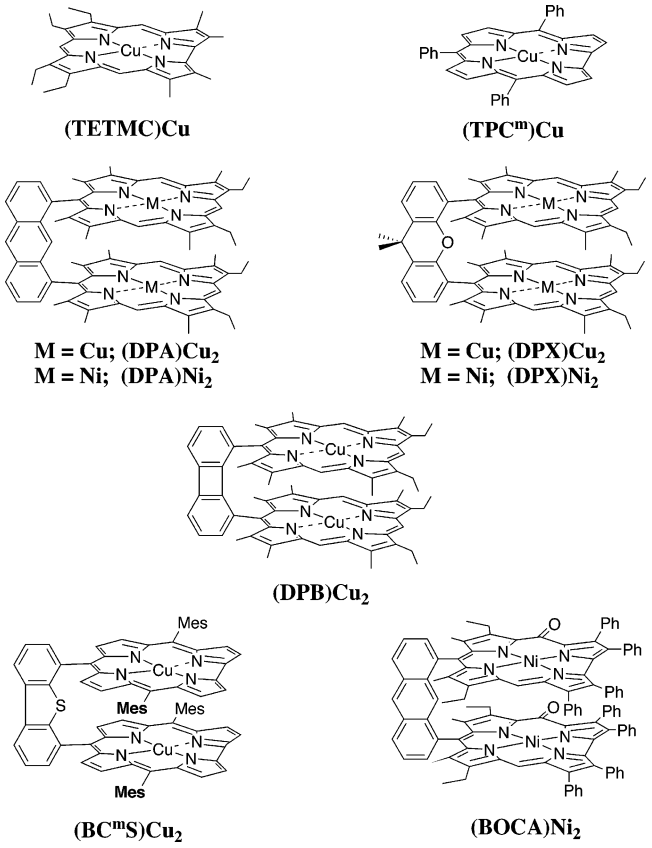

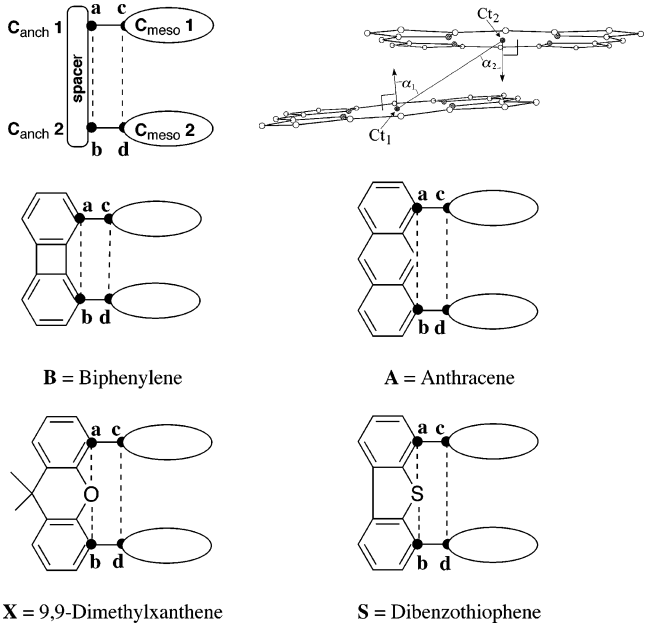

Figure 6. Series of aromatic linking units in this work and in the literature used to join corrole or porphyrin monomers to form the cofacial biscorrole or porphyrin−corrole dimers, where the a−b and c−d distances are defined. The other geometrical parameters are also defined.

(Table 2). In the $(BC^mS)Cu_2$ complex, where meso-aryl-substituted corroles are present,[64] the distances range from 1.88 to 1.90 Å, indicating slightly stronger interactions than those found in other reported corrole ligands. The coordination distances shown in the monometallic (TPC^m)-Cu complex, also incorporating a meso-aryl-substituted corrole, are within the range of values found for (BC^mS)-Cu_2. (In $(TPC^m)Cu$, the four Cu−N_{pyr} distances are 1.89 Å.[39]) The other metallocorrole complex described in the literature, namely (TETMC)Cu, exhibits the shortest copper−ligand

distances for these complexes (1.86−1.87 Å). All of the reported Cu−N_{pyr} bond lengths lie within the characteristic copper(III)−N(donor ligand) range of distances (1.804−1.907 Å),[59] supporting the existence of Cu(III) centers in the monometalated and bimetalated corrole copper complexes discussed above.

***π*−*π* or Metal−Metal Interactions.** In Figure 6, the distance between the macrocycle meso carbon 1 and meso carbon 2 and that of the spacer-anchored carbon 1 and anchored carbon 2 are defined as *d*(c−d) and *d*(a−b), respectively. Table 2 shows selected geometrical parameters derived from the molecular structures of (BCA)Cu_2, (BCB)Cu_2, and (PCB)Cu_2. The macrocyclic centers (Ct) were calculated as the centroids of the four nitrogen atoms belonging to each macrocycle. The interplanar angles (θ) were measured as the angle between the two macrocyclic least-squares mean planes (LSMPs). Plane separations were measured as the perpendicular distance from one macrocycle least-squares plane to the center of the other macrocycle; reported mean plane separations (MPS) were the average of the two plane separations for each dimer. The slip angles (α) were calculated as the angle between the vector joining the two macrocyclic centers and the unit vectors normal to the two macrocyclic least-squares planes ($\alpha = (\alpha_1 + \alpha_2)/2$, where α_i = angle(Ct−Ct, n_i), $i = 1, 2$). Lateral shift is defined as $L = d(\text{Ct}-\text{Ct}) \times \sin \alpha$.

The a−b distance (see Figure 6), which mainly depends on the spacer nature, is close to 3.79 Å for the biphenylene group in both (BCB)Cu_2 and (PCB)Cu_2 and close to 4.98 Å for the anthracene moiety of (BCA)Cu_2. Similar values (roughly ±0.01 Å) are given in the literature for other face-to-face complexes incorporating these spacers.[60,61,66] Molecular structures showing coordinated or inserted molecules in the complex cavity can lead to significant differences between the *d*(c−d) and *d*(a−b) distances, as is the case for the (BCA)Co_2 complex where $\Delta d_1 = d(\text{c}-\text{d}) - d(\text{a}-\text{b}) = 0.30$ Å.[42] This is also observed in (BCA)Cu_2 where a toluene solvent molecule is placed inside the cavity roughly parallel to both macrocycles (the dihedral angles between the macrocycles least-squares mean planes and that of the inserted molecule are 7.7° and 11.3°, respectively), leading to a difference of $\Delta d_1 = 0.28$ Å.

Steric interactions between substituents can also play a role in the positive values Δd_1. However, in both (BCB)Cu_2 and (PCB)Cu_2, where *d*(a−b) is shorter than in (BCA)Cu_2, repulsive interactions lead to important deformations in the macrocycles on the opposite side of the spacer (Figures 3 and 5) rather than induce an open-cavity geometry ($\Delta d_1 > 0$). In particular, it is noteworthy that the Δd_1 values calculated for (BCB)Cu_2 and (PCB)Cu_2 are equal to −0.01 and 0 Å, respectively. Indeed, considering these values along with both the short MPS distances (3.65 and 3.48 Å, respectively) and the small θ angles (9.2 and 5.3°) seems to indicate that an attractive interaction exists between the macrocycles in each complex. In addition, we note that the metal centers are slightly displaced from their respective ligand LSMP toward each other, the Cu−LSMP distances being close to 0.12/0.10 Å and 0.05/0.16 Å. For these complexes, the centroid−centroid distance (respectively, 4.13 and 3.73 Å) is ∼0.1 Å longer than the related copper−copper geometry (4.02 and 3.63 Å) (i.e., $\Delta d_2 < 0$ and equal to −0.11 and −0.10 for (BCB)Cu_2 and (PCB)Cu_2, respectively). Thus, all of these geometrical features indicate an interaction between both monometalated moieties in (BCB)Cu_2 and (PCB)Cu_2. In particular, it should be pointed out that, for these complexes, the short MPS geometries are not accompanied by large lateral shifts (L) between macrocycles, these two kinds of values being the signature of $\pi-\pi$ interactions only. Thus, along with the short MPS and M−M geometries, the low lateral shift values found for (BCB)Cu_2 and (PCB)Cu_2 ($L = 2.02$ and 1.49 Å, respectively) further support both $\pi-\pi$ and copper−copper interactions in the crystal. This contrasts with the case of (BCA)Cu_2, where a solvent molecule is located inside the complex cavity, and the Ct−Ct and M−M distances are large and similar to each other (6.34 and 6.35 Å, $\Delta d_2 = 0.01$ Å), thus indicating that the M−M interactions are weak in (BCA)Cu_2.

Similar geometrical trends are also found in (DPB)Cu_2 and (DPX)Cu_2 ($\Delta d_1 = 0$ and −0.27 Å, MPS = 3.50 and 3.60 Å, $\theta = 4.4$ and 4.6°, *d*(M−M) = 3.81 and 3.91 Å, $L =$ 1.63 and 1.74 Å, and $\Delta d_2 = d(\text{M}-\text{M}) - d(\text{Ct-Ct}) = -0.05$ and −0.07 Å, respectively). The latter case is particularly interesting due to the fact that the X spacer exhibits a *d*(a−b) distance (4.59 Å) greater than that of the three other examined complexes, (BCB)Cu_2, (PCB)Cu_2, and (DPB)Cu_2, which incorporate a biphenylenyl linking unit (*d*(a−b) = 3.79, 3.79, and 3.80 Å, respectively). The short M−M and MPS distances observed in (DPX)Cu_2 are because of deformation of the long X spacer, which folds on two equivalent halves through the O···C direction and leads to an angle of 165.9° between them. Thus, the *d*(a−b) distance in this complex is significantly shorter than the maximum allowed value for a planar conformation of the spacer (∼5.0 Å). This folding, along with the reported (DPX)Cu_2 geometrical parameters (which are close to those of (BCB)Cu_2, (PCB)Cu_2, and (DPB)Cu_2, despite the significant difference between their *d*(a−b) distances), supports an interaction between the macrocyclic moieties in (DPX)Cu_2 as pointed for the three other considered compounds.

The other two biscopper complexes included in Table 2, namely (BCA)Cu_2 and (BC^{m}S)Cu_2,[64] exhibit large M−M and MPS values and positive Δd_1 and Δd_2 differences. Although for the former compound this is due to the toluene solvent molecule inserted inside the complex cavity, the large Δd_1 (0.28 and 1.02 Å, respectively) and lateral shift values (1.02 and 4.87 Å, respectively) for the latter result from the presence of two methyl groups (each belonging to a mesityl moiety of one macrocycle) that are inside the complex cavity and are involved in C−H···M contacts. (With the hydrogen atoms placed at calculated positions, the observed *d*(H···M) distances are 2.58 and 2.66 Å.)

The three homobimetallic nickel complexes (DPX)Ni_2,[65] (BOCA)Ni_2,[45] and (DPA)Ni_2[63] present calculated negative

(66) Harvey, P. D.; Proulx, N.; Martin, G.; Drouin, M.; Nurco, D. J.; Smith, K. M.; Bolze, F.; Gros, C. P.; Guilard, R. *Inorg. Chem.* **2001**, *40*, 4134−4142.

Δd_1 and Δd_2 values as well as small interplanar angles (θ = 2.6, 7.8 and 3.9°) and short interplanar distances (MPS = 3.60, 4.29 and 3.87 Å, see Table 2). Although in $(DPA)Ni_2$ the metal−metal distance is slightly shorter than that found in $(DPX)Ni_2$ and in $(BOCA)Ni_2$ (4.57 Å compared to 4.69 and 4.68 Å, respectively), these two latter complexes exhibit an almost equivalent geometry despite both the different oxocorrolato ligand incorporated in $(BOCA)Ni_2$ (inhibiting partially the full delocalization of the electrons throughout the macrocycle) and the different spacer incorporated in $(DPX)Ni_2$, which does not fold as much as in $(DPX)Cu_2$ (6.4 compared to 14.1°, respectively). As in the case of the four homobimetallic copper complexes, $(BCB)Cu_2$, $(PCB)Cu_2$, $(DPB)Cu_2$, and $(DPX)Cu_2$, the similar molecular geometries found for these three quite different bisnickel complexes suggest $\pi-\pi$ or metal−metal interactions. By comparison of the MPS and the M−M distances calculated for both biscopper and bisnickel series, we systematically observe shorter geometries for the former complexes, indicating stronger interactions in the homobimetallic copper compounds. An inspection of the Δ(MPS) and Δ(M−M) differences observed between the complexes of both series shows that, in all cases, Δ(M−M) is greater than Δ(MPS), leading to the conclusion that the difference between Cu···Cu and Ni···Ni interactions is more important than that between their corresponding ligands.

Despite the absence of a linking spacer, it is noteworthy that the metallocorrole (TETMC)Cu crystallizes as a dimer,[59] showing two crystallographically independent copper corrole molecules in the dimer moiety. In the crystal structure of this compound, the macrocycles are planar (MDMP = 0.07/0.08 Å), the metal centers lying on the planes (M−LSPM = 0.05/0.03 Å). The interplanar distance (3.42 Å) is shorter and the interplanar angle is smaller (0.5°) than values observed in $(BCB)Cu_2$, $(PCB)Cu_2$, $(DPB)Cu_2$, and $(DPX)Cu_2$ (MPS = 3.65, 3.48, 3.50, and 3.60 Å, θ = 9.2, 5.3, 4.4, and 4.6°, respectively). In contrast, the metal−metal distance of the (TETMC)Cu dimer (4.72 Å) is significantly longer and its lateral shift value (3.40 Å) is larger than in the face-to-face bimetallic copper complexes reported in this study (d(Cu−Cu) = 4.02, 3.63, 3.81, and 3.91 Å, L = 2.02, 1.49, 1.63, and 1.74 Å, respectively). These geometrical features therefore suggest that (i) a mainly $\pi-\pi$ interaction takes place between the macrocycles of the $[(TETMC)Cu]_2$ dimer and (ii) a mainly weak interaction exists between the metal centers of this molecular unit. Weak metal−metal interactions are consistent with the lack of any detectable influence on the ESR and magnetic measurement data. However, the interactions between the two π systems must be strong as it is reflected in the electrochemistry of the dyads as discussed below.

Electrochemistry of Mono- and Bis-copper Corroles. The electrochemistry of the monomeric copper corrole, $(Me_4Ph_5Cor)Cu$, and the corresponding face-to-face copper biscorroles, $(BCA)Cu_2$ and $(BCB)Cu_2$ (see Chart 1), was examined in CH_2Cl_2 containing 0.1 M TBAP. The cyclic voltammograms for these compounds are illustrated in Figure 7 and the redox potentials are summarized in Table 4.

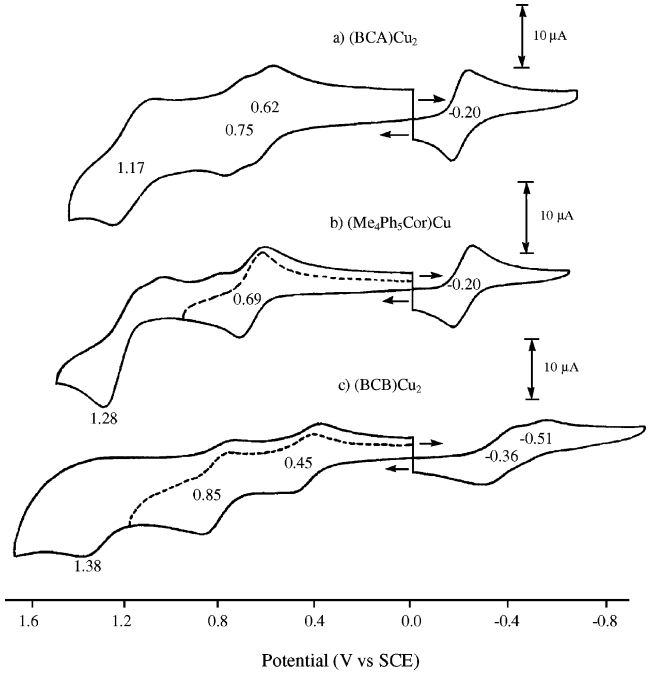

Figure 7. Cyclic voltammograms of (a) $(BCA)Cu_2$ (1.5×10^{-3} M), (b) $(Me_4Ph_5Cor)Cu$ (1.2×10^{-3} M), and (c) $(BCB)Cu_2$ (1.5×10^{-3} M) in CH_2Cl_2 containing 0.1 M TBAP. Scan rate = 0.1 V/s.

Table 4. Summary of Half-Wave Potentials[a]

metal ion	compound	oxidation		reduction
Cu	$(Me_4Ph_5Cor)Cu$	1.28[e]	0.69	−0.20
	$(BCA)Cu_2$	1.17	0.75 0.62	−0.20
	$(BCB)Cu_2$	1.38[e]	0.85 0.45	−0.36 −0.51
Co[b]	$(Me_4Ph_5Cor)Co$	0.72	0.47	−0.16
	$(BCA)Co_2$	0.89	0.47	−0.23
	$(BCB)Co_2$	0.83	0.44 0.27	−0.31 −0.60
Co[c]	$(MPA)Co$[f]		−0.06[e]	−1.53
	$(DPA)Co_2$		0.05	−1.60
	$(DPB)Co_2$		0.17 0.00	−1.71 −1.90
2H[d]	$(C_2diE)H_2$[g]	0.90	0.39	−1.81
	$(DPA)H_4$	0.85	0.43 0.31	−1.92
	$(DPB)H_4$	0.92	0.37 0.14	−2.06
Zn[d]	$(C_2diE)Zn$	0.63	0.22	−2.00
	$(DPA)Zn_2$	0.60	0.23 0.16	−2.11
	$(DPB)Zn_2$	0.85 0.64	0.21 0.06	−2.15

[a] Data obtained in CH_2Cl_2, 0.1 M TBAP for Cu complexes and in PhCN, 0.1 M TBAP for the reminder of the compounds. [b] From ref 42. [c] From ref 68. [d] From ref 70. [e] E_p for a scan rate of 0.1 V/s. [f] Monomeric cobalt porphyrin. [g] Monomeric free-base porphyrin.

The monocorrole, $(Me_4Ph_5Cor)Cu$, undergoes one reversible reduction (Figure 7b) at $E_{1/2}$ = −0.20 V; there are also two oxidations at $E_{1/2}$ = 0.69 V and E_{pa} = 1.28 V for a scan rate of 0.1 V/s. The reversible reduction, which is metal-centered,[30] results in the formation of $[(Me_4Ph_5Cor)Cu^{II}]^-$, and the reduction potential of −0.20 V is comparable to the $E_{1/2}$ values of −0.20 to −0.24 V for the reduction of the related Cu(III) triphenylcorroles, [T(*p*-X−P)Cor]Cu where X = H, CH_3, or OCH_3.[67] The reduction potential of $(Me_4Ph_5Cor)Cu$ is also anodically shifted by 140 mV as compared to that of (OEC)Cu where

(67) Wasbotten, I. H.; Wondimagegn, T.; Ghosh, A. *J. Am. Chem. Soc.* **2002**, *124*, 8104−8116.

$E_{1/2} = -0.34$ V under the same solution conditions. This shift in half-wave potential is consistent with a decreased basicity of $(Me_4Ph_5Cor)Cu$ as compared to (OEC)Cu and is analogous to what is seen when comparing the more difficult to reduce octaethylporphyrin (OEP) with tetraphenyl derivatives (TPP) having the same central metal ion.[4]

The first reduction and first oxidation of $(Me_4Ph_5Cor)Cu$ both involve a reversible one-electron transfer, and no evidence of dimerization is observed upon oxidation as is the case for (OEC)Cu.[30] In this regard, it should be pointed out that the triphenylcorroles [T(*p*-X−P)Cor]Cu (X = H, CH_3, or OCH_3) also show no evidence of dimerization.[67] From this result, it is clear that the substituents on the corrole macrocycle must have a significant effect on the electrooxidation mechanism.

The biscorrole complex, $(BCA)Cu_2$, undergoes three reversible oxidations in CH_2Cl_2 with $E_{1/2}$ values located at 0.62, 0.75, and 1.17 V. The formation of $[(BCA)Cu_2]^{2+}$ where each macrocycle is singly oxidized is split into two processes, and the potential separation between the two $E_{1/2}$ values is 130 mV. The peak currents of the first two oxidations are also both lower than that of the third oxidation or the first reduction, both of which involve the global abstraction or addition of two electrons, and this is thus comparable to what was reported for (OEC)Cu[30] whose first two oxidations occur via two stepwise one-electron abstractions from each macrocycle in the electrogenerated corrole $\pi-\pi$ dimer. The potential separation between the first two oxidations of (OEC)Cu is 140 mV, a value comparable to the 130 mV separation observed in the case of $(BCA)Cu_2$. However in contrast to what is seen for (OEC)-Cu, the monomeric corrole, $(Me_4Ph_5Cor)Cu$ with phenyl substituents does not dimerize during the first oxidation (Figure 7b).

The electrooxidation of $(BCB)Cu_2$ occurs in three steps, the first two of which are reversible and the result of a split oxidation for the formation of $[(BCB)Cu_2]^{2+}$ with $E_{1/2}$ values located at 0.45 and 0.85 V. The third oxidation is irreversible with $E_{pa} = 1.38$ V for a scan rate of 0.1 V/s. As in the case of $(BCA)Cu_2$, the first two oxidations of $(BCB)Cu_2$ can be assigned to a stepwise abstraction of one electron from each corrole macrocycle. The potential separation between the first two oxidations of $(BCB)Cu_2$ is 400 mV, a value much larger than in the case of $(BCA)Cu_2$ or (OEC)Cu where the potential separations are 130 and 140 mV, respectively.

The smaller potential separation between the first two oxidations of $(BCA)Cu_2$ as compared to that of $(BCB)Cu_2$ can be attributed to a smaller $\pi-\pi$ interaction between the two corrole macrocycles in the copper corroles with anthracene spacers, and this is similar to what was observed for the two related cobalt complexes, $(BCA)Co_2$ and $(BCB)Co_2$,[42] as well as other linked bisporphyrins[68] that also possess face-to-face macrocycles and the same two linking spacer groups (anthracenyl or biphenylenyl). These comparisons are summarized in Table 4.

The biscorroles and bisporphyrins that possess anthracene (A) as a spacer group both show weaker $\pi-\pi$ interactions as compared to those of the same macrocycles with biphenylene (B) as a spacer. Generally, these types of anthracene-bridged compounds show either no splitting at all in the first oxidation or a small degree of splitting, along with small potential separations between $E_{1/2}$ of the first two oxidations (Table 4). For example, neither $(BCA)Co_2$ nor $(DPA)Co_2$ shows a splitting of the first oxidation. $(DPA)H_4$ and $(DPA)Zn_2$ have a split first oxidation and a potential separation of 70−120 mV, which is smaller than in the case of $(DPB)H_4$ or $(DPB)Zn_2$ where the potential separation is 150−230 mV. The stronger interaction between two corrole macrocycles or the two porphyrin macrocycles with biphenylene (B) as a spacer is attributed to the shorter distance between the two linking carbons in the biphenylene group as compared to that in anthracene (A).

Because of the $\pi-\pi$ interaction, both corrole macrocycles in $(BCA)Cu_2$ and $(BCB)Cu_2$ are stepwise oxidized at different potentials as compared with the corresponding monomeric corrole, $(Me_4Ph_5Cor)Cu$. The monomer is oxidized at 0.69 V (Figure 7b), and when the wave is split, one process becomes easier and the other harder. This is shown in Figure 7a for the case of $(BCA)Cu_2$ and Figure 7c for the case of $(BCB)Cu_2$. Similar results have been reported for other face-to-face biscorroles[42] or bisporphyrins,[68] and the relevant electrochemical data are listed in Table 4.

The electroreduction of $(BCA)Cu_2$ in CH_2Cl_2, 0.1 M TBAP shows only one reversible reduction $E_{1/2} = -0.20$ V, and this leads to a formal Cu(II) species. The half-wave potential for this reaction is identical to $E_{1/2}$ for the reduction of the monomeric compound, $(Me_4Ph_5Cor)Cu$ (i.e., −0.20 V). In contrast, $(BCB)Cu_2$ undergoes two reversible reductions (a split process) with $E_{1/2}$ values located at −0.36 and −0.51 V (Figure 7c). The peak current for each reduction of $(BCB)Cu_2$ is smaller than the peak current for the single reduction of $(BCA)Cu_2$ or $(Me_4Ph_5Cor)Cu$ (Figure 7), consistent with a splitting of the reduction into two processes. The two reduction steps correspond to the stepwise addition of one electron to each of the two copper centers of the corrole unit. Both reductions of $(BCB)Cu_2$ also occur at more negative potentials than those for the reduction of monomeric $(Me_4Ph_5Cor)Cu$, consistent with a strong $\pi-\pi$ interaction in $(BCB)Cu_2$. Thus, as seen in Figure 7c, the half-wave potential of −0.20 V for reduction of $(Me_4Ph_5Cor)Cu$ shifts to −0.36 and −0.51 V for the reduction of $(BCB)Cu_2$. The same trend is seen in Table 4 for the electroreduction of the other face-to-face biscorroles or bisporphyrins that possess an anthracene (A) or biphenylene (B) spacer.

Electrochemistry of Porphyrin−Corrole Dyads. Cyclic voltammograms of the two porphyrin−corrole dyads, $(PCA)Cu_2$ and $(PCB)Cu_2$, in CH_2Cl_2 containing 0.1 M TBAP are illustrated in Figure 8, which includes for comparison voltammograms for the two monomeric units, $(Me_4Ph_5Cor)Cu$ and $(Me_2Et_6PhP)Cu$. The electrochemistry of $(Me_2Et_6PhP)Cu$ is virtually identical to that of (OEP)Cu under the same solution conditions. $(Me_2Et_6PhP)Cu$ undergoes one reversible reduction at $E_{1/2} = -1.49$ V and two

(68) Le Mest, Y.; L'Her, M.; Collman, J. P.; Kim, K.; Hendricks, N. H.; Helm, S. *J. Electroanal. Chem.* **1987**, *234*, 277−295.

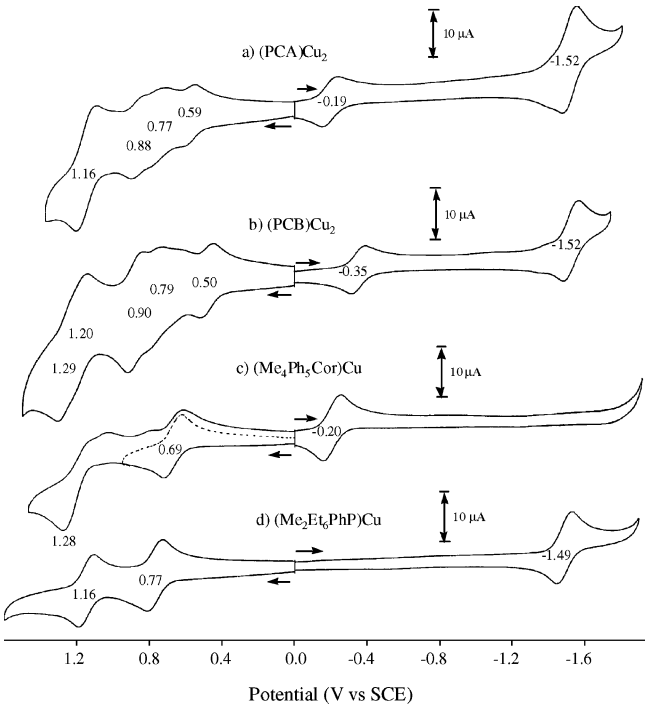

Figure 8. Cyclic voltammograms of (a) $(PCA)Cu_2$ (1.5×10^{-3} M), (b) $(PCB)Cu_2$ (1.3×10^{-3} M), (c) $(Me_4Ph_5Cor)Cu$ (1.2×10^{-3} M), and (d) $(Me_2Et_6PhPor)Cu$ (1.2×10^{-3} M) in CH_2Cl_2 containing 0.1 M TBAP. Scan rate = 0.1 V/s.

reversible oxidations at $E_{1/2} = 0.77$ and 1.16 V. (OEP)Cu undergoes one reversible reduction at $E_{1/2} = -1.53$ V and two reversible oxidations at $E_{1/2} = 0.77$ and 1.25 V. Each redox process is assigned as occurring at the porphyrin π-ring system leading to the formation of a π-anion radical upon reduction and a π-cation radical and dication upon oxidation.[69]

The porphyrin−corrole dyads, $(PCA)Cu_2$ and $(PCB)Cu_2$, both undergo two well-defined reductions within the cathodic potential limit of CH_2Cl_2. The reduction potentials are located at $E_{1/2} = -0.19$ and -1.52 V for $(PCA)Cu_2$ and at $E_{1/2} = -0.35$ and -1.52 V for $(PCB)Cu_2$. The first electron addition occurs at the copper center of the corrole ring, and the second, at the π-ring system of the porphyrin. The latter $E_{1/2}$ value is comparable to that for the monomeric porphyrin, $(Me_2Et_6PhP)Cu$.

The half-wave potential for the first reduction of $(PCA)Cu_2$ (-0.19 V vs SCE) is almost the same as that of the monomeric corrole unit, $(Me_4Ph_5Cor)Cu$, and the bis-corrole, $(BCA)Cu_2$, both of which are located at $E_{1/2} = -0.20$ V. However, like $(BCB)Cu_2$, the $(PCB)Cu_2$ complex is also harder to reduce than the monomeric unit, and the single reduction shifts cathodically to $E_{1/2} = -0.35$ V. Again, as in the case of $(BCB)Cu_2$, the negative shift of $E_{1/2}$ may be attributed to an increased $\pi-\pi$ interaction between the two macrocycles. This leads to a harder reduction in the case of those compounds with B spacers (as opposed to A spacers) and is demonstrated for $(BCA)Co_2$ versus $(BCB)Co_2$[42] and $(DPA)Co_2$ versus $(DPB)Co_2$[70] (Table 4).

The electrochemical oxidation of the two porphyrin complexes is characterized by four and five well-defined one-electron processes for $(PCA)Cu_2$ and $(PCB)Cu_2$, respectively. The half-wave potentials are located at 0.59, 0.77, 0.88, and 1.16 V for $(PCA)Cu_2$, the latter of which involves two overlapping one-electron-transfer processes (Figure 8a). The oxidation potentials of $(PCB)Cu_2$ are located at 0.50, 0.79, 0.90, 1.20, and 1.29 V. Five electrooxidations are also observed when benzonitrile or tetrahydrofuran is used as the solvent (data not shown).

Spectroelectrochemistry of Biscorrole Complexes and Porphyrin−Corrole Dyads. Figure 9, parts a−c, gives a spectral comparison between the neutral (−) and singly reduced (- - -) forms of the different copper corroles. $(Me_4Ph_5Cor)Cu$, $(BCA)Cu_2$, and $(BCB)Cu_2$ each exhibit an intense Soret band at 404−410 nm and a broad, weak visible band located at 569−570 nm (Table 5). Upon reduction, the Soret band is red-shifted and located at 426 nm for $(Me_4Ph_5Cor)Cu$, 421 nm for $(BCA)Cu_2$, and 423 nm for $(BCB)Cu_2$. In each case, an intense visible band close to 600 nm is observed for the electrogenerated Cu(II) product. This type of visible band is not seen in any monomeric Cu(II) porphyrin (e.g., (OEP)Cu or $(Me_2Et_6PhPor)Cu$ (see Table 5)) and can thus be considered as a "marker band" for the electrogenerated Cu(II) corroles.

Further proof for the stepwise addition of one electron to each copper center of $(BCB)Cu_2$ is given by ESR spectra taken during electroreduction of the compound in CH_2Cl_2, 0.2 M TBAP (Figure 10). The ESR spectrum of neutral $(BCB)Cu_2$ shows an extremely weak signal in agreement with a bis-Cu(III) representation of the complex along with a small contribution of a bis-Cu(II) radical species as discussed above in the ESR section. However, upon controlled potential reduction of $(BCB)Cu_2$ at -0.45 V to generate $[(BCB)Cu_2]^-$, a well-defined ESR spectrum is obtained ($g_{\|} = 2.151$; $g_{\perp} = 2.038$) whose features are characteristic of a copper(II) porphyrin-like species (Figure 10a). Further reduction at -0.70 V leads to the formation of $[(BCB)Cu_2]^{2-}$ with no change in the shape of the ESR signal ($g_{\|} = 2.155$; $g_{\perp} = 2.043$) in accordance with the formation of the bis-copper(II) species (Figure 10b). The signal is not a triplet, indicating little or no interaction between the two Cu(II) centers in the reduced complex.

The two neutral $(PCA)Cu_2$ and $(PCB)Cu_2$ complexes have similar UV−vis spectral characteristics as seen in Figure 9, parts d and e. $(PCA)Cu_2$ has a strong Soret band at 407 nm and two visible bands at 531 and 566 nm. $(PCB)Cu_2$ has a strong Soret band at 401 nm and two visible bands at 528 and 564 nm (Table 5 and Figures 9, parts d and e). These spectral features can be compared to those of the monomeric porphyrin, $(Me_2Et_6PhPor)Cu$, which has bands at 407, 530, and 566 nm. A comparison may also be made to (OEP)Cu, which has bands at 401, 526, and 562 nm. However, despite a similarity in λ_{max} for all of the above compounds, it must be pointed out that the molar absorptivities (ϵ) of the Soret band in $(PCA)Cu_2$ and $(PCB)Cu_2$ are only about half those of the monomeric porphyrins, $(Me_2Et_6PhPor)Cu$ and (OEP)Cu (Table 5). The ϵ values of the Soret band in

(69) Kadish, K. M. *Prog. Inorg. Chem.* **1986**, 435−605.
(70) Le Mest, Y.; L'Her, M.; Hendricks, N. H.; Kim, K.; Collman, J. P. *Inorg. Chem.* **1992**, *31*, 835−847.

Table 5. UV-Visible Spectral Data of Cu Complexes in Nonaqueous Solvents with the Cu(II) Corrole ≪Marker Band≫ Located in the Range 594−604 nm

solvent	macrocycle	compound	λ_{max}, nm ($\epsilon \times 10^{-4}$, M^{-1} cm^{-1})						
			neutral species			singly reduced species at corrole center			
CH_2Cl_2	corrole	$(Me_4Ph_5Cor)Cu$	410 (10.1)	569 (1.7)		426 (12.6)		552 (1.7)	594 (6.0)
	biscorrole	$(BCA)Cu_2$	410 (13.0)	570 (2.5)		421 (15.4)		553 (2.6)	595 (6.0)
	biscorrole	$(BCB)Cu_2$	404 (11.8)	570 (2.1)		423 (12.2)		558 (4.3)	598 (7.7)
PhCN	corrole	$(Me_4Ph_5Cor)Cu$	416 (8.9)	574 (1.5)		430 (11.6)		557 (1.5)	597 (5.5)
	porphyrin	$(Me_2Et_6PhP)Cu$	407 (38.4)	530 (1.5)	566 (2.2)				
	porphyrin	(OEP)Cu	401 (34.5)	526 (1.3)	562 (2.9)				
	PC[a]	$(PCA)Cu_2$	407 (19.0)	531 (1.9)	566 (2.3)	407 (19.2)	531 (1.9)	566 (2.3)	599 (2.2)
	PC[a]	$(PCB)Cu_2$	401 (18.6)	528 (1.7)	564 (2.0)	401 (18.4)	528 (1.7)	564 (2.0)	604 (1.5)
			singly oxidized species			doubly oxidized species			
CH_2Cl_2	corrole	$(Me_4Ph_5Cor)Cu$	410 (7.4)	532 (0.7)	569 (0.5)				
	biscorrole	$(BCA)Cu_2$	410 (11.7)	550 (1.8)	570 (1.8)	416 (9.5)	570 (1.1)		
	biscorrole	$(BCB)Cu_2$	404 (10.5)		573 (1.3)	398 (10.5)	880 (1.5)		

[a] PC = porphyrin−corrole.

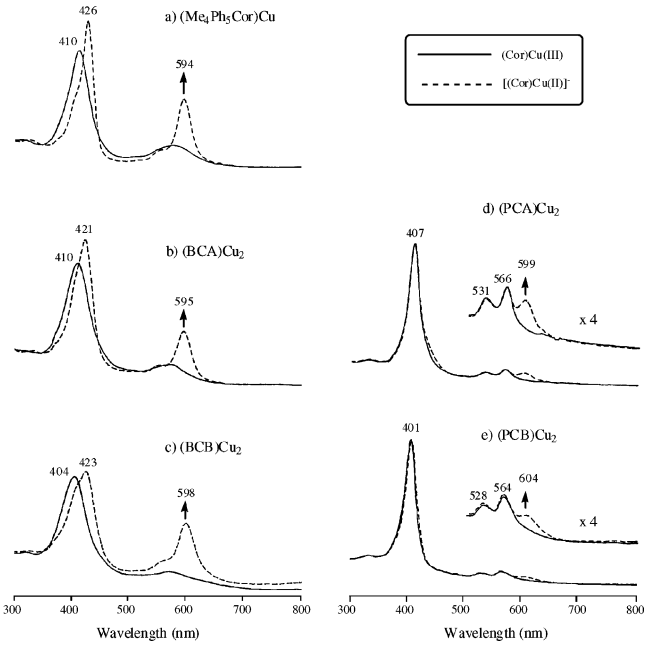

Figure 9. Spectral comparison between neutral Cu(III) species (−) and electrogenerated Cu(II) species (- - -) for (a) $(Me_4Ph_5Cor)Cu$, (b) $(BCA)Cu_2$, and (c) $(BCB)Cu_2$ in CH_2Cl_2, 0.2 M TBAP, and (d) $(PCA)Cu_2$ and (e) $(PCB)Cu_2$ in PhCN, 0.2 M TBAP.

$(Me_2Et_6PhPor)Cu$ and (OEP)Cu are 38.4×10^4 and 34.5×10^4 M^{-1} cm^{-1}, respectively, as compared to 19.0×10^4 M^{-1} cm^{-1} for $(PCA)Cu_2$ and 18.6×10^4 M^{-1} cm^{-1} for $(PCB)Cu_2$. Thus, the spectral characteristics of the corrole unit in $(PCA)Cu_2$ and $(PCB)Cu_2$ are not readily observable because of the much stronger intensity of the porphyrin bands that dominate the UV−vis spectrum of the molecule (Table 5).

The spectral changes upon the first reduction of $(PCA)Cu_2$ and $(PCB)Cu_2$ in PhCN, 0.2 M TBAP are shown in Figure 9, parts d and e. The Soret band of both complexes undergoes no change upon the first reduction, but a well-defined visible band around 600 nm appears for the singly reduced species. As in the case of the monomer, this band is characteristic of the formation of a Cu(II) corrole product. This result clearly indicates that the first reduction of both $(PCA)Cu_2$ and $(PCB)Cu_2$ involves the copper

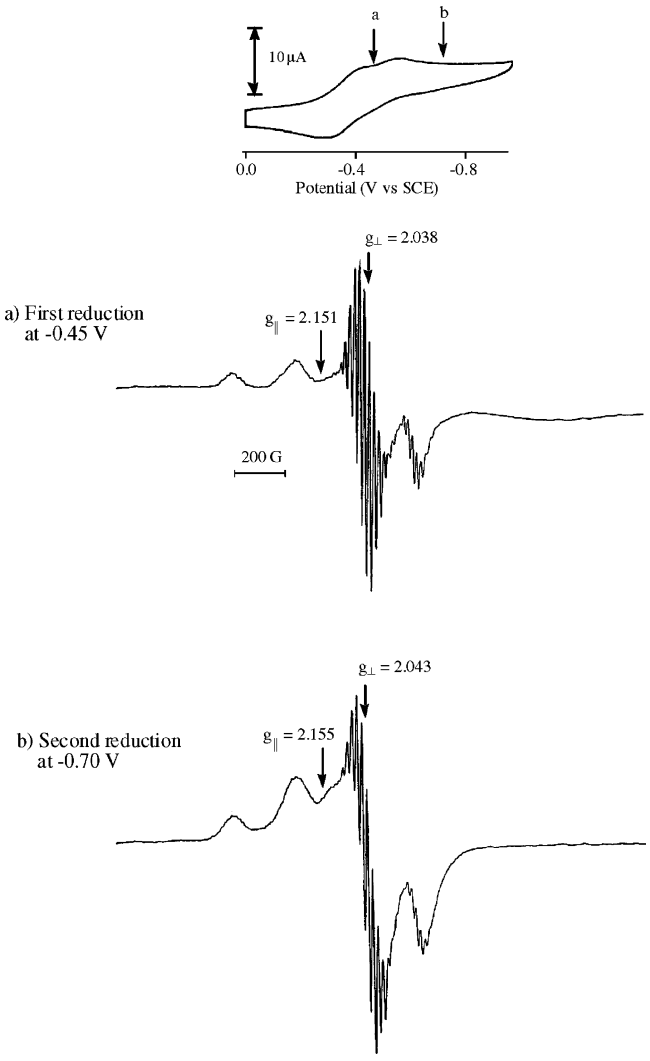

Figure 10. ESR spectra during the electroreduction of $(BCB)Cu_2$ leading to (a) $[(BCB)Cu_2]^-$ and (b) $[(BCB)Cu_2]^{2-}$ at 120 K in CH_2Cl_2, 0.2 M TBAP.

center of the corrole and not the porphyrin unit, and this leads to the formation of a bis-Cu(II) complex (i.e., $(Por)Cu^{II}-[(Cor)Cu^{II}]^-$).

UV−vis spectroelectrochemistry was also carried out for oxidation of the three corroles in CH_2Cl_2, 0.2 M TBAP. The corresponding spectral changes are illustrated in Figure 11,

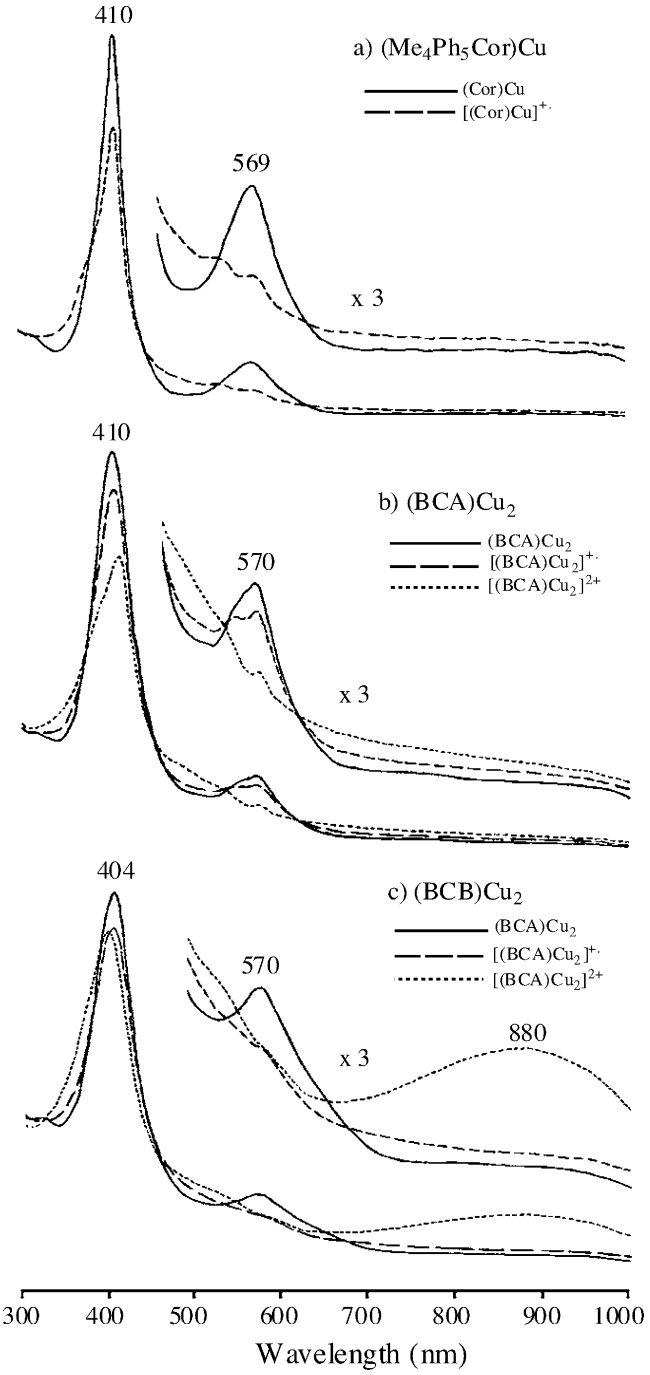

Figure 11. Spectral comparison of copper corroles between neutral species and the singly or doubly oxidized species for (a) $(Me_4Ph_5Cor)Cu$, (b) $(BCA)Cu_2$, and (c) $(BCB)Cu_2$ in CH_2Cl_2, 0.2 M TBAP.

and the data are collected in Table 5. Neutral (Me_4Ph_5Cor)-Cu (−) has bands at 410 and 569 nm, and these both decrease in intensity upon the first oxidation, suggesting the abstraction of an electron from the π system of the corrole.[30] The same result is seen in Figure 11b upon the first (- - -) and second (···) oxidations of $(BCA)Cu_2$ where the Soret and visible bands both decrease in intensity.

As discussed in the electrochemistry section, the first and second oxidations of $(BCA)Cu_2$ involve a stepwise abstraction of one electron from each corrole macrocycle, and this leads to the formation of a π-cation radical and dication (Figure 11b and Table 5). The spectral changes upon the first oxidation of $(BCB)Cu_2$ (Figure 11c) are characterized by decreased intensity Soret and visible bands, similar to what is seen for $(Me_4Ph_5Cor)Cu$ and $(BCA)Cu_2$. However, the doubly oxidized corrole displays a blue shift in the Soret band (with respect to the singly oxidized species), and the wavelength changes from 404 to 398 nm along with the appearance of a new broad visible band centered at 880 nm. A similar near-IR band was observed at 890 nm for $[(OEC)Cu]_2^+$ and at 820 nm for $[(OEC)Ni]_2^+$.[30] This band is observed only in $(BCB)Cu_2$ in the biscorrole series and may be attributed to a strong $\pi-\pi$ interaction existing in the case of $[(BCB)Cu_2]^{2+}$. This result is consistent with electrochemical results discussed in the previous section.

Conclusions

A comparative study of four cofacial copper bis-corrole (BC) and porphyrin−corrole (PC) dyads and their related monomeric corrole and porphyrin units shows that electronic interaction between the two face-to-face macrocycles of these cofacial derivatives depends critically on the type and size of the rigid spacer. For the investigated bismacrocycles, the copper corrole macrocycle in a face-to-face configuration with another copper corrole or copper porphyrin can be considered as a Cu(III) complex in equilibrium with a Cu(II) radical, the copper(III) species being the main oxidation state of the corrole at all temperatures as clearly evidenced by ^{1}H NMR studies. X-ray crystallographic data suggests weak metal−metal interactions, and this is consistent with the lack of any detectable effect on the ESR or magnetic measurement data. However, the electrochemistry of the dyads shows clearly that a strong $\pi-\pi$ interaction exists between the two macrocycles of $(BCB)Cu_2$ as compared to those of $(BCA)Cu_2$, the dimer that has a larger interplanar distance between the two macrocycles.

Acknowledgment. The support of the Robert A. Welch Foundation (K.M.K., Grant E-680) and the French Ministry of Research, CNRS (UMR 5633) is gratefully acknowledged. The Région Bourgogne and Air Liquide company are acknowledged for scholarships (F.J.), and we are also grateful to M. Soustelle for the synthesis of pyrrole and dipyrromethane precursors. N. Kiritsakas (Université Louis Pasteur, Strasbourg, France) is acknowledged for the resolution of the X-ray structure of $(BCA)Cu_2$.

Supporting Information Available: Crystallographic data of $(BCB)Cu_2$, $(BCA)Cu_2$, and $(PCB)Cu_2$, ESR spectra (100 K and room temperature) of $(BCA)Cu_2$, $(PCA)Cu_2$, $(BCB)Cu_2$, and $(PCB)Cu_2$. This material is available free of charge via the internet at http://pubs.acs.org.

IC049651C